Langmuir

Research Article

Hybridization at a Surface: The Role of Spacers in DNA Microarrays

A. Halperin, A. Buhot, and E. B. Zhulina

Langmuir, **2006**, 22 (26), 11290-11304• DOI: 10.1021/la0616606 • Publication Date (Web): 03 November 2006

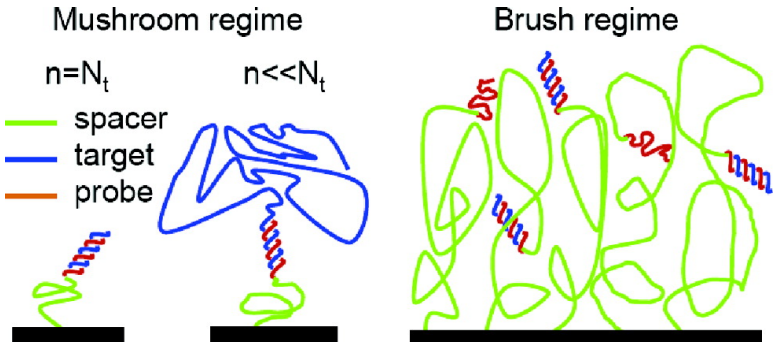

More About This Article

Additional resources and features associated with this article are available within the HTML version:

- Supporting Information
- Links to the 1 articles that cite this article, as of the time of this article download
- Access to high resolution figures
- Links to articles and content related to this article
- Copyright permission to reproduce figures and/or text from this article

View the Full Text HTML

Langmuir is published by the American Chemical Society. 1155 Sixteenth Street N.W., Washington, DC 20036

Hybridization at a Surface: The Role of Spacers in DNA Microarrays

A. Halperin* and A. Buhot

Structures et Propriétés d'Architectures Moléculaires, UMR 5819 (CEA, CNRS, UJF), DRFMC/SPrAM, CEA-Grenoble, 38054 Grenoble Cedex 9, France

E. B. Zhulina

Institute of Macromolecular Compounds of the Russian Academy of Sciences, 199004 St Petersburg, Bolshoy Prospect 31, Russia

Received June 9, 2006. In Final Form: September 11, 2006

Flexible spacer chains are utilized to enhance the hybridization of terminally anchored oligonucleotide probes of DNA microarrays. A polymer physics approach identifies an underlying mechanism and yields guidelines for the optimal spacer length in terms of the effect on the equilibrium state. For low grafting densities, the dominant effect arises because of the decimation in the number of accessible chain configurations due to the impenetrable surface. Opposing trends are found for long targets and for short targets. At higher grafting densities, different brush regimes introduce an extra hybridization penalty. A novel brush regime is obtained for long neutral spacers and short targets at intermediate ionic strength where the chain stretching is due to the electrostatic interactions between the probes.

I. Introduction

Hybridization at interfaces allows one to interrogate multicomponent solutions of nucleic acids, NA, comprising NA of different sequences called targets. In DNA microarrays, probes of single stranded (ss) DNA of known sequence are placed at specific sites, "spots". When contacted with the solution, the probes (p) preferentially hybridize with free NA targets (t), incorporating the complementary sequence. The degree of hybridization at the different spots provides information on the composition of the solution.[1−5] It is useful to distinguish between two common formats of DNA microarrays or "chips". cDNA chips are based on long cDNA probes physisorbed onto a solid support. Oligonucleotide microarrays utilize short ss oligonucleotide probes that are terminally anchored, chemically grafted, to the surface. The sensitivity of DNA chips is clearly dependent on the efficiency of hybridization at the surface. For oligonucleotide microarrays, the efficiency of hybridization at the surface can be enhanced by introducing spacer chains to attach the terminus of the probe to the grafting site.[6−8] These create distance between the probes and the impenetrable surface, thus approaching the hybridization conditions of free chains in solution. While the beneficial role of spacers is generally recognized, a coherent view of their optimal design and of the underlying physics is yet to emerge. This situation is apparent from the large number of reported protocols for preparation and functionalization of surfaces for DNA chips. It is also evident from the diverging conclusions of experimental studies of spacer efficiency. For example, some report benefits only for long targets, while others observed enhanced hybridization also for short ones.

The theoretical analysis we present below is an initial step toward a unified picture of the role of spacers. It yields guidelines for the optimization of the spacer length based on its effect on the equilibrium of the hybridization reaction at an impenetrable, planar surface. The discussion aims to clarify the interplay of the following design parameters: (i) the number of bases in a probe, n; (ii) the number of bases in a target, N_t; (iii) the number of monomers in the spacer, N_s; and (vi) the area per probe site, Σ. Our analysis utilizes polymer physics methodology focusing on the role of two physical factors. One is the reduction of the number of accessible chain trajectories upon grafting to an impenetrable planar surface. This effect is especially significant when interactions between the probes, hybridized or not, are weak. Such is the case for low surface densities of probes and at higher densities when the hybridization degree, x_{eq}, is low. The second effect is the formation of a polymer brush because of the crowding of the spacer chains anchoring the probes and the associated interaction free energy penalty. For brevity, we limit the discussion to neutral flexible spacers grafted to a nonadsorbing planar surface and to solutions containing a single type of ssDNA targets. This last condition eliminates competitive hybridization reactions from our analysis. The oligonucleotide probes are grafted to surface sites activated by linkers, allowing chemical coupling to the terminus of the probes. We distinguish between short monomeric linkers with $N_s \gtrsim 1$ and long chain linkers, spacers, with $N_s \gg 1$. Our analysis focuses on the equilibrium state of the surface hybridization reaction

$$\mathrm{sp} + \mathrm{t} \rightleftharpoons \mathrm{spt} \qquad (1)$$

when the unhybridized probes, sp, are anchored via long spacers. To clarify the effect of the spacers, we compare this reaction to the one involving probes anchored via short linkers with $N_s \gtrsim 1$, $\mathrm{p} + \mathrm{t} \rightleftharpoons \mathrm{pt}$. A second useful reference is the bulk hybridization reaction of free chains in solution $\mathrm{p(free)} + \mathrm{t} \rightleftharpoons \mathrm{pt(free)}$, where p(free) is a free ssDNA probe and pt(free) is its free hybridized form. Our analysis concerns two regimes. In one, the surface density of the probes is sufficiently low so as to ensure negligible interactions between neighboring probes, hybridized or not, i.e., $\Sigma^{1/2}$ is large compared to the range of interactions between the sites. In this large Σ regime, the hybridization isotherm of $\mathrm{sp} + \mathrm{t} \rightleftharpoons \mathrm{spt}$ assumes a Langmuir form relating the equilibrium

* Corresponding author.

(1) Graves, D. J. *Trends Biotechnol.* **1999**, *17*, 127−134.
(2) Wang, J. *Nucleic Acids Res.* **2000**, *28*, 3011−3016.
(3) Heller, M. J. *Annu. Rev. Biomed. Eng.* **2002**, *4*, 129−153.
(4) Lockhart, D. J.; Winzeler, E. A. *Nature (London)* **2000**, *405*, 827−836.
(5) Levicky, R.; Horgan, A. *Trends Biotechnol.* **2005**, *23*, 143−148.
(6) Pirrung, M. C. *Angew. Chem., Int. Ed.* **2002**, *41*, 1277−1289.
(7) Southern, E.; Mir, K.; Shchepinov, M. *Nat. Genet.* **1999**, *21*, 5−9.
(8) Heise, C.; Bier, F. F. *Top. Curr. Chem.* **2006**, *261*, 1−25.

10.1021/la0616606 CCC: $33.50
Published on Web 11/03/2006

hybridization fraction x_{eq} to the concentration of the targets, c_t,

$$\frac{x_{eq}}{1 - x_{eq}} = c_t K_{spt}. \quad (2)$$

Here, the equilibrium constant $K_{spt}(N_s, n, N_t)$ depends on the spacer length N_s. It differs from the hybridization isotherm of p + t ⇌ pt where K_{spt} is replaced by $K_{pt}(n, N_t)$. As expected, $K_{spt}(N_s, n, N_t)$ approaches its bulk value as N_s increases. However, as we shall see, the variation with N_s depends on the length of the target, N_t. For short targets, $K_{spt}(N_s, n, N_t)$ decreases when N_s increases, while an opposite trend is predicted for long targets. These two opposing trends are obtained for $N_s \gg 1$. They reflect the asymptotic behavior of the number of accessible chain trajectories of terminally anchored chains at an impenetrable surface. Importantly, this result does not allow for local steric effects at the grafting site. Within our approach, this last contribution can only be discussed qualitatively by assuming a plausible form for the steric effect. As we shall discuss, this suggests that the variation of K_{spt} with N_s exhibits a maximum when $N_t = n$. In contrast, K_{spt} increases monotonically for $N_t \gg n$. The second case we discuss concerns one of the possible small Σ regimes where probe−probe interactions play an important role. A number of such scenarios are possible, depending on the ionic strength as well as the values of N_s, N_t, and n. In high-ionic-strength solutions, the interactions are due to the brush formation because of the crowding in the probe layer. These give rise to a modified form of the hybridization isotherm

$$\frac{x_{eq}}{1 - x_{eq}} = c_t K_{spt} \exp[-\Gamma(x_{eq})] \quad (3)$$

Here, $\Gamma(x_{eq})$ reflects the interaction penalty incurred by a target hybridizing at the surface. The various cases differ with respect to the form of $\Gamma(x_{eq})$. Two scenarios involving short linkers were studied earlier. For short targets such that $N_s \ll N_t = n$, the hybridization reaction gives rise to a mixed polyelectrolyte brush of double stranded (ds) DNA and ssDNA. When the probes comprise $n \approx 15$ bases, the brush thickness is only weakly dependent on x_{eq} and $\Gamma(x_{eq}) = \text{const}(1 + x_{eq})$.[9] A different $\Gamma(x_{eq})$ is obtained when the targets are much longer than the probes, $N_s \ll n \ll N_t$, and the hybridization gives rise to a polyelectrolyte brush comprising flexible, nonhybridized ssDNA tails of the pt.[10] In this case, the brush thickness varies with x_{eq} and $\Gamma(x_{eq}) = \text{const}(x_{eq}^{2/3} - x_B^{2/3})$, where x_B specifies the threshold of tail overlap. In the following, we will consider a third case involving long spacers carrying short oligonucleotide probes and hybridizing with targets of equal length i.e., $N_s \gg N_t = n$. In this system, an additional novel regime appears, characterized by $\Gamma(x_{eq}) = \text{const}\cdot(1 + x_{eq})^{1/3}$. It reflects the lowering of the electrostatic interaction penalty, incurred upon hybridization at the surface, by stretching the neutral spacers.

In addition to its relevance to the design of DNA chips and the understanding of hybridization at a surface, this theory problem is of interest from the perspectives of both polymer and surface sciences. Grafted chains and polymer brushes attracted considerable attention within the polymer science community.[11−13] The study of these systems focused primarily on grafted homopolymers. In contrast, the hybridization at the surface exhibits three novel features. First, it involves grafted block copolymers. A probe anchored via a spacer, denoted here as sp, is a coil−coil diblock copolymer. Second, the architecture of the grafted chains changes upon hybridization with the target, t. When $N_t = n$, the configuration of the unhybridized sp changes into a coil−rod diblock spt because the flexible ssDNA block turns into a rigid dsDNA domain. An spt coil−rod−coil triblock copolymer is obtained when the targets are long, $N_t \gg n$. In this case, the rigid dsDNA domain carries a tail of ssDNA. Finally, the brush characteristics vary significantly with the hybridization degree as determined by the bulk concentration of the targets, c_t. This last tuning parameter has no counterpart in "conventional" brushes. From the surface science perspective, the associated hybridization isotherms are of interest because they are, in fact, adsorption isotherms modified to allow for the polymeric character of the adsorbing species as well as the adsorption sites.

In Section II, we will discuss the general features of our model in the context of the existing experiments and of different possible theoretical approaches. The experimental results will be summarized in view of identifying the accessible range of parameters and specifying the regimes captured by our model. The capabilities and limitations of our approach are then discussed in comparison with alternative theoretical methods. The effect of the impenetrable wall on the hybridization behavior of sparsely grafted probe layers is analyzed in Section III. The analysis is based on known results concerning the number of configurations of chains tethered to a planar impenetrable surface. A scaling description of mixed brushes comprising sp and spt chains is presented in Section IV. It is based on the Alexander model,[14] assuming a steplike concentration profile and uniformly stretched chains. A novel hybridization regime occurs when the interactions between the neutral spacer monomers are negligible in comparison to the electrostatic interactions between the probes, hybridized or not. The corresponding self-consistent field (SCF) theory is discussed in Section V. It allows one to calculate the concentration profiles of the monomers and the free ends. The concentration profiles associated with the novel hybridization regime differ qualitatively from the familiar ones, as obtained for brushes of flexible homopolymers. For the cases where we analyzed the SCF theory, it supports the conclusions of the scaling approach.

II. Experimental and Theoretical Background

Two experimental studies, by Shchepinov et al.[15] and by Guo et al.,[16] reported the effect of systematic variation of the spacer length on the fold change of the hybridization signal. Shchepinov et al. utilized regular copolymer spacers comprising phosphate groups joined by short hydrocarbon or poly(ethylene oxide) (PEO) chains. Varying the length of the joining chains within the copolymers controlled their charge density. The role of charges was further probed by addition of positive side groups to the bridging chains. Spacers of up to 30 repeat units were studied. The longest spacers were roughly comparable to PEO chains of $N_s \approx 40$. In this study, the probes were hybridized with short targets, $N_t = n = 12$. As expected, higher electrical charge density was detrimental to the hybridization. However, the authors concluded that the spacer length is the dominant design parameter. Importantly, this study revealed a nonmonotonic effect of the spacer length. The hybridization signal initially increased with the spacer length. Maximal hybridization intensity was observed for spacers comprising 8−10 repeat units. A further increase in

(9) Halperin, A.; Buhot, A.; Zhulina, E. B. *Biophys. J.* **2004**, *86*, 718−730.
(10) Halperin, A.; Buhot, A.; Zhulina, E. B. *Biophys. J.* **2005**, *89*, 796−811.
(11) Milner, S. T. *Science* **1991**, *251*, 905−914.
(12) Halperin, A.; Tirrell, M.; Lodge, T. P. *Adv. Polym. Sci.* **1992**, *100*, 31−71.
(13) Rühe, J. et al. *Adv. Polym. Sci.* **2004**, *165*, 79−150.
(14) Alexander, S. *J. Phys. (Paris)* **1977**, *38*, 983−987.
(15) Shchepinov, M. S.; Case-Green, S. C.; Southern, E. M. *Nucleic Acids Res.* **1997**, *25*, 1155−1161.
(16) Guo, Z.; Guilfoyle, R. A.; Thiel, A. J.; Wang, R.; Smith, L. M. *Nucleic Acids Res.* **1994**, *22*, 5456−5465.

the spacer length led to a lower hybridization degree. A smaller range of spacer lengths of different chemistry was reported by Guo et al. who utilized dT spacers comprising $N_s = 0$, 3, 6, 9, 12, and 15 bases. Upon hybridization with long targets, $n = 15 \ll N_t = 157$, they observed a monotonic increase in hybridization signal with the length of the spacers for $N_s \geq 9$. The signal obtained for shorter spacers was virtually nonexistent. On the basis of their results, the authors suggested that further gains in hybridization strength may be attained by using longer spacers. The hybridization was carried at 0.75 M of NaCl. Useful additional information is reported by Beattie et al.,[17] Livache et al.,[18] and Joos et al.[19] Beattie et al. utilized a probe of length of $n = 9$ anchored via spacers of different lengths. The spacers incorporated up to seven triethylglycol phosphoryl residues or mixed chains of triethylglycol phosphoryl and dT of up to 18 units. Fold changes in the hybridization efficiency as a function of the spacer length were not reported. However, the authors concluded that spacer chains do not enhance the hybridization efficiency of PCR products comprising $N_t \leq 300$ bases but may facilitate the capture of longer PCR products. The hybridization was carried out with 0.9 M NaCl. Livache et al. examined the effect of dT spacers on the hybridization efficiency of polypyrrole oligonucleotide chips with $n = 15$ probes and long targets with $N_t = 165$ in a hybridization solution containing 0.5 M of NaCl. Spacers comprising 3, 5, and 10 dT units were tried out, leading to the conclusion that spacers comprising 5 or more dT enhanced the hybridization. Finally, Joos et al. found that 15 base oligonucleotide spacers increased the efficiency of the hybridization of probes with $n = 35$ to short targets with $N_t = 70$ in a solution containing 0.3 M NaCl.

The following points are important for our subsequent discussion:

(i) Two chemical strategies were utilized in the experiments cited. Both involve stepwise addition of monomers. In one, oligonucleotide spacers were incorporated into the sequence of a presynthesized probe prior to the grafting to the surface.[16−19] In the second strategy, of Shchepinov et al.,[15] the spacers were synthesized in situ. In this last case, the spacer monomers were chosen because of the yield of the in situ synthesis. PEO spacers were not utilized because of the low yield of the reaction for spacers longer than EO_6. The synthetic feasibility of such spacers was, however, demonstrated earlier by Maskos and Southern.[20] It is supported by recently reported synthesis of oligonucleotide−PEO diblock copolymers.[21−23]

(ii) While the current practice favors hybridization solutions with 1 M NaCl, the experiments cited explored solutions of lower ionic strength in the range 0.3−0.9 M NaCl.

(iii) Some experiments utilized short targets, $N_t = n$, while others utilized long ones, $N_t \gg n$. None studied the variation of the spacer effects with the length of the target.

(vi) The effect of spacer was gauged by monitoring the hybridization signal after a given time. Equilibrium was not established, and the saturation hybridization signal was not measured. It is, thus, difficult to distinguish clearly between effects due to transport or kinetics and those resulting from modification of the equilibrium state. This rules out quantitative interpretation of the experiments cited earlier in terms of hybridization isotherms.

Our analysis of the spacer effects utilizes a polymer physics approach assuming that the spacers, the probes, and the targets may be considered as long chains. This approach yields simple analytical expressions for $K_{spt}(N_s, n, N_t)$ and $\Gamma(x_{eq})$. In turn, these provide insights on the physical origins of the spacer benefits and guidelines for the choice of the spacer length. However, this is achieved at a price of coarse graining the chemical structure and limiting the discussion to relatively long spacers. It is useful to elaborate on this issue because of its importance for comparison with experiments and with alternative theoretical methods. In the long-chain approximation we adopt, both the spacers and the ssDNA blocks are viewed as chains of freely jointed Kuhn segments described by their asymptotic behavior. Depending on the chain rigidity, each Kuhn segment may correspond to several monomers. For a chain characterized by a persistence length l, the number of monomers of size a in the Kuhn segment is roughly $p \approx 2l/a$. As noted, the analysis utilizes the asymptotic behavior of the chains. A freely jointed chain with no excluded volume interactions approaches the asymptotic behavior of a Gaussian chain for $N = 4$ Kuhn segments.[24] The chemical structure of the chains, bond angles, and lengths, as well as steric or strain effects, is absorbed into l and a. Accordingly, our model does not quantitatively describe short chains, incorporating 2−3 Kuhn segments, because the asymptotic behavior is not attained. It may, however, capture qualitative aspects of this range. In contrast, this model cannot describe the behavior of short linkers of a length comparable to the Kuhn segment, that is, when the number of monomers in the linker is in the range $0 < N_s/p_s < 1$. In this case, the freely jointed chain model is not applicable and the detailed chemical structure of the linker plays a key role.

Within the polymer physics approach we utilize, interactions between monomers are characterized by virial coefficients corresponding to binary monomer−monomer interactions. To describe an sp chain, it is, thus, necessary to introduce three virial coefficients υ_s, υ_p, and υ_{sp}, allowing, respectively, for interactions between the spacer monomers, between the probe monomers, and between the spacer and probe monomers. When the monomers are electrically neutral, the virial coefficient assumes the form

$$\upsilon \simeq a^3(1 - \theta/T) \tag{4}$$

where T is the temperature and θ is the theta temperature. This form allows for the interplay of hard core repulsion and long-range van der Waals attraction. The interactions between charged monovalent monomers in solutions of high ionic strength are described by[10]

$$\upsilon \simeq a^3(1 - \theta/T) + l_B r_D^2 \tag{5}$$

Here, $l_B = e^2/\epsilon kT$ is the Bjerrum length, k is the Boltzmann constant, $r_D = 1/\sqrt{8\pi l_B c_{salt}}$ is the Debye length corresponding to a 1:1 salt of concentration c_{salt}, ϵ is the T-dependent dielectric constant of water, and e is the elementary charge. The second term reflects the electrostatic interactions between two impenetrable, singly charged spheres in a strongly screened solution as given by the Debye form of the Poisson−Boltzmann equation. The virial coefficients, as cited above, do not allow for the role of water structure or possible electrostatic correlations. Also, the values of the phenomenological parameters a, l, and θ for the

(17) Beattie, K. L. et al. *Clin. Chem.* **1995**, *41*, 700−706.
(18) Livache, T. et al. *Anal. Biochem.* **1998**, *255*, 188−194.
(19) Joos, B.; Kuster, H.; Cone, R. *Anal. Biochem.* **1997**, *247*, 96−101.
(20) Maskos, U.; Southern, E. M. *Nucleic Acids Res.* **1992**, *20*, 1679−1684.
(21) Cha, T.-W.; Boiadjiev, V.; Lozano, J.; Yang, H.; Zhu, X.-Y. *Anal. Biochem.* **2002**, *311*, 27−32.
(22) Ameringer, T.; Hinz, M.; Mourran, C.; Seliger, H.; Groll, J.; Moeller, M. *Biomacromol.* **2005**, *6*, 1819−1823.
(23) Schlapak, R.; Pammer, P.; Armitage, D.; Zhu, R.; Hinterdorfer, P.; Vaupel, M.; Frühwirth, T.; Howorka, S. *Langmuir* **2006**, *22*, 277−285.
(24) Flory, P. J. *Statistical Mechanics of Chain Molecules*, 2nd ed.; Carl Hanser Verlag: Munich, Germany, 1989.

spacers as well as for the ssDNA are not well-established. For ssDNA, $a_p \approx 6$ Å is cited,[25,26] while the reported values of the persistence length vary in the range of 7.5 Å $\leq l_p \leq$ 35 Å[27] and θ_p is currently unknown. In the range of interest, the dsDNA is a rodlike molecule with each base contributing $b = 3.4$ Å to its total length.[28,29] The parameters of the heteropolymer spacers used by Shchepinov et al. were not studied; however, some are known for PEO homopolymers where the monomer size is $a_s \approx$ 3 Å[30] and the persistence length is $l_s = 9$ Å.[31] Finally, within our analysis, the surface is planar, impenetrable, and nonadsorbing. It is assumed to be laterally uniform, and its atomic structure is not taken into account.

Relief of steric factors was invoked in the discussion of spacer effects.[7,15,16] The term "steric effects" usually refers to the interplay between nonbonded van der Waals repulsion between substituent groups and the resulting combination of bond angle strain, bond stretches, and bond compressions.[32] In the present context, it is useful to distinguish between three types of steric effects. The simplest is steric crowding upon hybridization at the surface. The hybridized probes form impenetrable cylinders of radius 9.5 Å. Complete hybridization of all probes is impossible because of steric hindrance when the spacers are short and the area per probe is lower than the cross-sectional area of a dsDNA, 284 Å^2. We will not consider this effect and limit the discussion to $\Sigma \geq$ 284 Å^2. A second possible effect may arise because of the geometry imposed by the linker to the surface. For example, a tilted orientation of the hybridized probe with respect to the impenetrable surface may give rise to steric hindrance to hybridization. This kind of effects involves the $0 < N_s/p_s < 1$ range and is outside the scope of our model. In our discussion, we will allow for the rough qualitative feature of this effect by assuming that K_{spt} increases with N_s in the range $0 < N_s/p_s < 1$. The steric effect our model does reflect is the impenetrability of the surface, i.e., the distance between the surface and a monomer cannot be smaller than a. This is described within the long-chain approximation via the number of allowed chain configurations where bond strain effects are not involved.

As stressed in the Introduction, the polymer science approach captures the asymptotic properties of the system. It cannot describe the effect of short spacers. Despite this limitation, this method is of interest because it yields simple transparent results and physical insights concerning the function of the spacers. Its merits are highlighted further upon comparison to two alternative theoretical approaches. The first involves an all-atom simulation of the system incorporating the detailed chemical structure of the surface, the linkers, the probes, and the targets. Such a simulation also allows for the interaction potentials among all ingredients, including the surrounding water molecules. An exploratory study of this type was recently reported by Wong and Pettitt[33] who performed an all-atom molecular dynamics simulation of 12 base-pair pt attached to an epoxy-coated glass surface by a short amine linker. Importantly, this 40 ns simulation did not allow one to characterize the equilibrium state. The authors estimated that a simulation time longer by a factor of 10−100 will be necessary in order to achieve this end. Such computational approaches promise to provide, eventually, detailed data on the hybridization behavior at the surface. It should be especially useful in studying short linkers when the "long-chain" approximation is inapplicable. However, it is important to note the inherent difficulties involved: First, the conclusions thus obtained depend on the choice of potentials used to describe the various ingredients: water molecules, DNA, surface, etc. Second, while the output of such a simulation may eventually reproduce reality, it does not translate in a simple way into design guidelines. Finally, the computational time needed in order to simulate systems involving longer chains is likely to remain unfeasible. This is especially the case when considering hybridization between long probes and long targets. The second alternative approach is a phenomenological model proposed by Vainrub and Pettitt (VP).[35−37] The VP approach is designed so as to utilize exact results, obtained by Ohshima and Kondo,[38] on the electrostatic interaction free energy between a penetrable charged sphere and an impenetrable charged surface in the strong screening regime when the Debye−Hückel approximation is applicable. Within it, one calculates the excess free energy of a probe layer incorporating xN_T hybridized probes, $G_{el}(x)$, with respect to an unhybridized layer comprising N_T probes. In effect, $G_{el}(x)$ is the sum of the contributions of xN_T hybridization events, $G_{el} = \sum_{i=1}^{xN_T} G_i(\sigma_i)$, each occurring at a different surface charge density $\sigma_i = \sigma_0 + in/A$, where A is the surface area of the spot. At each step, the probe layer is modeled as a planar charged surface interacting with a *single* penetrable charged sphere. The ith hybridization step experiences a charge density σ_i reflecting uniform smearing of the electrical charges of all other probes, hybridized or not. In the VP model, the associated free energy term is $G_i(\sigma_i) = G_{pt}(\sigma_i) - G_p(\sigma_i)$ where G_{pt} (G_p) is the electrostatic free energy of a pt (p) sphere in contact with a planar layer of charge density σ_i. The VP approach relies on a prescription for assigning an effective charged sphere to the p and pt chains. It cannot be extended to describe the hybridization at lower ionic strength when the Ohshima and Kondo result does not apply. Furthermore, the VP approach focuses on electrostatic interactions while ignoring the configurations of the chains. In particular, the dimensions of the spheres corresponding to p or pt chains do not vary with Σ or x. Accordingly, this model cannot account for the chain extension as encountered in the brush regimes for $N_t \gg n > N_s$ and $N_s \gg n$, when the thickness of the probe layer changes with Σ and x. It is also difficult to extend the VP prescription for assigning an effective sphere to p and pt chains in the case of probes bound via long neutral spacers.

III. Sparsely Grafted Probes: Spacer and Surface Effects

The number of accessible chain configurations is reduced when a polymer is terminally anchored to an impenetrable surface such as a glass slide. Accordingly, the entropies of both the reactants and the products of the surface hybridization reaction are lowered with respect to their bulk values. This affects the equilibrium of the p + t ⇌ pt reaction, whose equilibrium constant K_{pt} differs from K_{bulk}, the equilibrium constant of the bulk hybridization reaction p(free) + t ⇌ pt(free). Flexible spacer

(25) Smith, S. B.; Cui, Y. J.; Bustamante, C. *Science* **1996**, *271*, 795−799.
(26) Strick, T. R.; Dessinges, M.-N.; Charvin, G.; Dekker, N. H.; Allemand, J.-F.; Bensimon, D.; Croquette, V. *Rep. Prog. Phys.* **2003**, *66*, 1−45.
(27) Mills, J. B.; Vacano, E.; Hagerman, P. J. *J. Mol. Biol.* **1999**, *285*, 245−257.
(28) Bloomfield, V. A.; Crothers, D.; Tinoco, I., Jr. *Nucleic Acids: Structures, properties and functions*; University Science Books: Sausalito CA, 2000.
(29) Cantor, C. R.; Schimmel, P. R. *Biophysical Chemistry*; W. H. Freeman: New York, 1980.
(30) Harder, P.; Grunze, M.; Dahint, R.; Whitesides, G. M.; Laibinis, P. E. *J. Phys. Chem. B* **1998**, *102*, 426−436.
(31) Kawaguchi, S.; Imai, G.; Suzuki, J.; Miyahara, A.; Kitano, T.; Ito, K. *Polymer* **1997**, *38*, 2885−2891.
(32) McNaught, A. D.; Wilkinson, A. *IUPAC Compendium of Chemical Terminology*, 2nd ed.; Blackwell Science: Cambridge, MA, 1997.
(33) Wong, K.-Y.; Pettitt, B. M. *Biopolymers* **2004**, *73*, 570−578.
(34) Adamson, A. W. *Physical Chemistry of Surfaces*, 4th ed.; J. Wiley: New York, 1982.
(35) Vainrub, A.; Pettitt, B. M. *Chem. Phys. Lett.* **2000**, *323*, 160−166.
(36) Vainrub, A.; Pettitt, B. M. *Phys. Rev. E* **2002**, *66*, 041905(4).
(37) Vainrub, A.; Pettitt, B. M. *Biopolymers* **2003**, *68*, 265−270.
(38) Ohshima, H.; Kondo, T. *J. Colloid Interface Sci.* **1993**, *157*, 504−508.

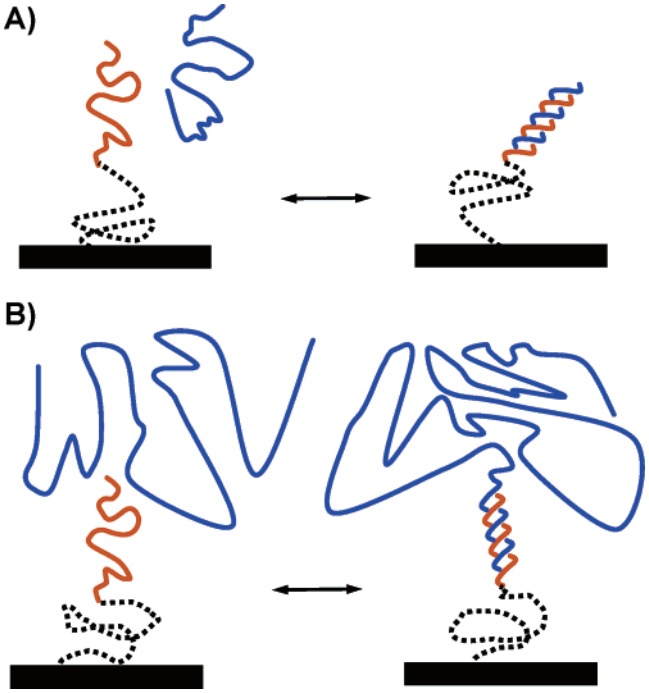

Figure 1. (A) Mushroom of spacer−probe (the spacer is depicted as a dotted line) diblock transforms into a coil−rod diblock upon hybridization to a short target of length identical to that of the probe. (B) When the target is long, it transforms into a coil−rod−coil triblock mushroom.

chains weaken the effect of the impenetrable wall. As a result, the equilibrium constant of the sp + t ⇌ spt reaction, K_{spt}, approaches K_{bulk} when $N_s \to \infty$. To quantify these statements, we aim to characterize K_{pt} and K_{spt} and compare them to K_{bulk}. Each equilibrium constant is specified by $K = \exp(-\Delta G^\circ/RT)$, where ΔG° is the corresponding standard hybridization free energy, $\Delta G^0 = G^0$ (products) $- G^0$ (reactants) and R is the molar gas constant. In turn, G_i^0 of each species, i = p, sp, pt, spt, or t, is related to the corresponding single-chain partition function Z_i via $G_i^0 = RT \ln Z_i$. Accordingly, $K_{pt} = Z_{pt}/Z_pZ_t$ and $K_{spt} = Z_{spt}/Z_{sp}Z_t$, while $K_{bulk} = Z_{pt}(\text{free})/Z_p(\text{free})Z_t$. The wall effects manifest themselves in the Z_i of the surface anchored species, i = p, pt, sp, and spt. They are, thus, most evident in

$$\frac{K_{pt}}{K_{bulk}} = \frac{Z_{pt}}{Z_{pt}(\text{free})}\frac{Z_p(\text{free})}{Z_p} \quad \text{and} \quad \frac{K_{spt}}{K_{bulk}} = \frac{Z_{spt}}{Z_{pt}(\text{free})}\frac{Z_p(\text{free})}{Z_{sp}} \tag{6}$$

Before we discuss the detailed derivation of these ratios and the underlying assumptions, it is helpful to present the main results and their physical origins. Importantly, the behavior of both K_{pt}/K_{bulk} and K_{spt}/K_{bulk} depend strongly on the target length N_t. For the simplest case of ideal chains behaving as random walks,

$$\frac{K_{pt}}{K_{bulk}} \sim \begin{cases} n^{1/2} \\ \left(\frac{n^3}{N_t}\right)^{1/2} \end{cases} \quad \text{and} \quad \frac{K_{spt}}{K_{bulk}} \sim \begin{cases} \left(\frac{N_s + n}{N_s}\right)^{1/2} & N_t = n \\ \left(\frac{N_s + n}{N_s + N_t - n}\right)^{1/2} & N_t \gg n \end{cases} \tag{7}$$

$K_{pt} > K_{bulk}$ when $N_t = n$ because the entropy of the anchored p chain is reduced because of the impenetrable surface while the entropy of the rodlike pt is only weakly affected (Figure 1A). The reactants are destabilized, thus shifting the equilibrium toward the products. In contrast, for $N_t \gg n$, two additional effects are involved. First, the pt chain is now a rod−coil diblock copolymer because of the long ssDNA tail attached to the rigid dsDNA domain (Figure 1B). The entropy of this tail is reduced by the vicinity of the surface. However, this effect is weakened since the rodlike dsDNA domain places the rod−tail junction at a distance above the surface. As a result, both $K_{pt} > K_{bulk}$ and $K_{pt} < K_{bulk}$ are possible. The second occurs for very long targets, $N_t > n^3$, when the entropy loss of the pt tails overwhelms that of the p chains. As expected, the spacer chains weaken the wall effects and K_{spt}/K_{bulk} approaches unity as N_s increases. This ratio decreases when $N_t = n$ but may either decrease or increase for $N_t > n$.

With this overall picture in mind, we now describe the analysis beginning with a summary of the underlying assumptions. Our discussion addresses the effect of the impenetrable surface in its pure form, that is, when there is no crowding between the chains and no adsorption to the surface. As we shall see, the length of the target has a qualitative effect on the variation of K_{spt} with N_s. For brevity, we will model both the spacer and the ssDNA as freely jointed chains with no excluded volume interactions. In other words, both chains behave as random walks (RW) rather then self-avoiding random walks (SAW). We will further assume that the number of monomers per Kuhn length is identical in the two chains i.e., $p_p = 2l_p/a_p = 2l_s/a_s = p_s = 1$. To allow for $p_p \neq p_s \neq 1$, it is only necessary to replace N_s, n, and N_t in the following equations by N_s/p_s, n/p_p and N_t/p_p. However, since the relevant parameters are currently unknown, the gain in generality does not compensate for the cumbersome form of the resulting equations. Assuming that the oligonucleotides and the spacers behave as RW is reasonable for the relatively short chains considered. Notice, however, that eq 5 yields $\upsilon_p > 0$. The effect of SAW statistics will be briefly considered at the end of the section. As we shall see no qualitative change is involved. Notice further that the asymptotic formulas we utilize do not enable us to consider blocks characterized by different θ temperatures.

The key ingredient in our discussion is the reduction in the number of accessible chain configurations at the vicinity of an impenetrable planar wall. This is apparent upon comparison of the asymptotic form of the partition function Z of free chains[39]

$$Z_{free}(N) = \bar{z}^N N^{\gamma - 1} \tag{8}$$

and of terminally anchored, nonoverlapping chains known as "mushrooms"[40,41]

$$Z_{mush}(N) = \bar{z}^N N^{\gamma_s - 1} \tag{9}$$

For an ideal chain behaving as a RW, $\bar{z}$ is identical to z_0, the coordination number of the lattice, $\gamma = 1$, and $\gamma_s = {}^1/_2$. For a SAW, $\bar{z} = \tilde{z} < z_0$, $\gamma = 1.167$, and $\gamma_s = 0.695$. A similar reduction is expected for rodlike molecules. The rotational partition function of a free rod, whose ends can explore the envelope of a sphere, is

$$Z_{rot}^{free} \sim 4\pi \tag{10}$$

In contrast, a rod with one end freely jointed to an impenetrable planar surface can only explore part of a hemisphere, thus leading to

(39) De Gennes, P. G. *Scaling Concepts in Polymer Physics*; Cornell University Press: Ithaca, NY, 1979.
(40) Duplantier, B. *J. Stat. Phys.* **1989**, *54*, 581−680.
(41) Eisenriegler, E.; Kremer, K.; Binder, K. *J. Chem. Phys.* **1982**, *77*, 6296−6320.

$$Z_{rot}^{surf} = \beta Z_{rot}^{free} \tag{11}$$

with $\beta \leq {}^1/_2$. For a freely rotating rod of zero thickness, $\beta = {}^1/_2$ since it can explore the whole hemisphere. In contrast to the flexible chain, the reduction in Z_{rot} of an anchored rod is independent of its length.

The partition functions of the free chains are well-known. $Z_p(\text{free}) = z_0^n$, $Z_t = z_0^{N_t}$, and $Z_{pt}(\text{free}) = z_0^{N_t+n} \exp(-\Delta G_{bulk}/RT)$. ΔG_{bulk} allows for the loss of configurational entropy of the hybridizing ssDNA, base pairing, initiation, etc. It also reflects the rotational entropy of the rodlike dsDNA domain, $S_{rot}^{free} = R \ln Z_{rot}^{free}$ where Z_{rot}^{free} is the corresponding rotational partition function. This last contribution is modified when the chains are tethered to the surface and it is convenient to introduce $\Delta\tilde{G}_{bulk}^0 = \Delta G_{bulk}^0 + TS_{rot}^{free}$, thus allowing us to rewrite $Z_{pt}(\text{free}) = z_0^{N_t+n} \exp(-\Delta\tilde{G}_{bulk}^0/RT) Z_{rot}^{free}$ and $K_{bulk} = \exp(-\Delta\tilde{G}_{bulk}^0/RT) Z_{rot}^{free}$. For sufficiently short probes, roughly $n \leq 20$, ΔG_{bulk}^0 is well-approximated by ΔG_{NN}^0 as obtained from the nearest-neighbor (NN) method.[42] ΔG_{NN}^0 is calculated by summing the contributions of nearest-neighbor base pairs allowing for an initiation term and the effect of dangling ends. $\Delta H_{NN}^0 = H_{init} + \sum_{i=1}^{n} \Delta H_i$ and $\Delta S_{NN}^0 = S_{init} + \sum_{i=1}^{n} \Delta S_i$ where the experimentally obtained ΔH_i and ΔS_i are the contributions of the $(i, i+1)$ base pair.

The discussion of K_{pt} requires two additional partition functions, Z_p and Z_{pt}. The first, as immediately specified by eq 9, is $Z_p = z_0^n n^{-1/2}$. The form of Z_{pt} depends, however, on the relative sizes of p and t. For $N_t = n$, the pt pair behaves as a rigid rod and the reduction in number of configurations is due solely to the effect of the wall on the rotational partition function. In this case,

$$Z_{pt} = z_0^{2n} \exp(-\Delta\tilde{G}_{bulk}^0/RT) \beta Z_{rot}^{free} \tag{12}$$

and

$$K_{pt} = \beta n^{1/2} K_{bulk} \tag{13}$$

For long targets $N_t \gg n$, the effect of the wall manifests itself primarily in the reduction of the number of states of the nonhybridized tail of pt. In this case, the end of the flexible ssDNA is not directly attached to the surface, as in the case of the p chains. Rather, it is attached to the end of a rodlike dsDNA segment. This creates a distance between the tail and the solid support, thus diminishing the surface effect. It is now necessary to distinguish between two situations, depending on the length of the rod, bn, as compared to the span of the flexible tail $R_0 = a_p(N_t - n)^{1/2}$. When $N_t > n + (bn/a_p)^2$ or $R_0 > bn$, the tail interacts with the surface for all rod orientations. On the other hand, when $n \leq N_t \leq n + (bn/a_p)^2$ or $R_0 \leq bn$, some rod orientations place the tail at altitudes larger than its own span. For these orientations, the interactions between the tail and the surface are negligible (Appendix A). Overall,

$$\frac{Z_{pt}}{Z_{pt}(\text{free})} = \begin{cases} \beta\left(1 - \dfrac{a_p\sqrt{N_t - n}}{2bn}\right) & \text{for } n \leq N_t \leq n + (bn/a_p)^2 \\ \dfrac{\beta bn}{2a_p\sqrt{N_t - n}} & \text{for } N_t > n + (bn/a_p)^2 \end{cases} \tag{14}$$

and

$$\frac{K_{pt}}{K_{bulk}} = \begin{cases} \beta n^{1/2}\left(1 - \dfrac{a_p\sqrt{N_t - n}}{2bn}\right) & \text{for } n \leq N_t \leq n + (bn/a_p)^2 \\ \dfrac{\beta bn^{3/2}}{2a_p\sqrt{N_t - n}} & \text{for } N_t > n + (bn/a_p)^2 \end{cases} \tag{15}$$

These expressions, for Z_{pt} and for K_{pt}, merge at $N_t = n + (bn/a_p)^2$ and reduce to eq 13 for the case $N_t = n$. Importantly, $K_{pt} < K_{bulk}$ when $N_t > n + (\beta b/2a_p)^2 n^3$. The hybridization of short targets is favored because the impenetrable surface reduces the entropy of the reactants, the probes, thus favoring the products whose entropy is only weakly reduced. The opposite trend can be found for long targets when the reduction in the entropy of the ss tails of pt dominates over the reduction of the entropy of the unhybridized probes, p.

Introducing flexible spacers requires modification of Z_p and Z_{pt}. When the spacer−probe sp behaves as a single flexible chain with $p_s = p_p = 1$,

$$Z_{sp} = z_0^{N_s+n}(N_s + n)^{-1/2} \tag{16}$$

For $n = N_t$, the partition function of the hybridized probe, Z_{spt}, is of a rodlike dsDNA segment attached to the surface by a flexible chain (Appendix A),

$$Z_{spt} = \beta_{av} z_0^{N_s+2n} K_{bulk} N_s^{-1/2} \tag{17}$$

Here, β_{av} is the average value of $\beta(y)$ defined by the rotational partition function of a rod with an end at height y via $Z_{rot}(y) = \beta(y) Z_{rot}^{free}$. β_{av} exhibits a slight N_s dependence increasing from $\beta_{av}(N_s = 1) = \beta$ to $\beta_{av}(N_s \gg 1) = 1$. The corresponding equilibrium constant is

$$K_{spt} = \beta_{av}\left(\frac{N_s + n}{N_s}\right)^{1/2} K_{bulk} \tag{18}$$

and the ratio to the bulk constant thus scales as $K_{spt}/K_{bulk} \approx [(N_s + n)/N_s]^{1/2}$. In the limit of $N_s \to \infty$, the ratio $K_{spt}/K_{bulk} \to 1$. At $N_s = n$, the ratio $K_{spt}/K_{bulk} \approx \sqrt{2}$. Thus, inasmuch as the asymptotic behavior is concerned, K_{spt}/K_{bulk} decreases as N_s increases and the spacers play a negative role. Importantly, the opposite trend is found when $N_t \gg n$. In this case (Appendix A),

$$Z_{spt} = z_0^{N_s+2n} K_{bulk}(N_s + N_t - n)^{-1/2} \tag{19}$$

where we have neglected the effect of the short hybridized domain on Z_{spt}. As a result,

$$K_{spt} = \left(\frac{N_s + n}{N_s + N_t - n}\right)^{1/2} K_{bulk} \tag{20}$$

The ratio $K_{spt}/K_{bulk} \approx [(N_s + n)/(N_s + N_t - n)]^{1/2}$ approaches unity when $N_s \to \infty$. At $N_s = N_t \gg n$, the ratio $K_{spt}/K_{bulk} \approx 1/\sqrt{2} \approx 0.7$. Thus, the ratio K_{spt}/K_{bulk} increases with N_s. The spacer effect is, thus, beneficial, though onset of saturation occurs roughly at $N_s = N_t$ and the utilization of longer spacers does not yield significant advantages (Figure 2).

The results obtained above require modification if the chains behave as SAW rather than RW. The resulting effect on the ratio of the equilibrium constants at the surface and in the bulk is,

(42) SantaLucia, J.; Hicks, D. *Annu. Rev. Biophys. Biomol. Struct.* **2004**, *33*, 415−450.

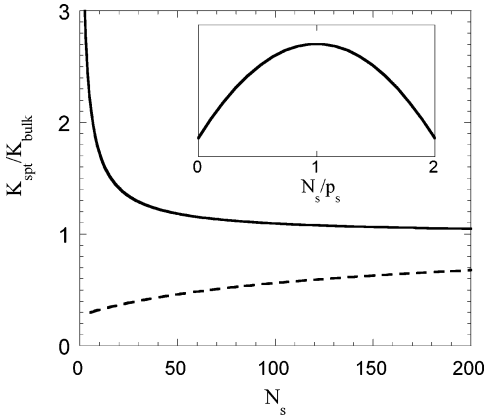

Figure 2. Effect of the spacers in the sparse grafting mushroom regime is evident from the plots of K_{spt}/K_{bulk} vs N_s. The asymptotic, $N_s \gg 1$, behavior is decreasing for short targets (—), eq 18, with $n = N_t = 20$ and β_{av} set to 1 but increasing for long targets (- - -), eq 20, with $n = 20$ and $N_t = 200$. Inset: A qualitative plot of K_{spt}/K_{bulk} vs N_s/p_s for $N_s/p_s \leq 2$. The combination of the spacer effects on the steric strain at the grafting site and the asymptotic effect of the impenetrable wall leads to a nonmonotonic behavior for short targets.

however, rather weak. To illustrate this point, consider the p(free) + t $\rightleftharpoons$ pt(free) and p + t $\rightleftharpoons$ pt reactions for $N_t = n$ when the ssDNA behaves as a SAW denoting the corresponding partition functions and equilibrium constants by $\tilde{Z}$ and $\tilde{K}$. For the bulk reaction, $\tilde{Z}_p(\text{free}) = \tilde{z}^n n^{\gamma-1}$ and $\tilde{Z}_t = \tilde{z}^n n^{\gamma-1}$ with $\gamma = 1.167$ while $\tilde{Z}_{pt}(\text{free}) = Z_{pt}(\text{free}) = z_0^{2n} K_{bulk}$, thus leading to $\tilde{K}_{bulk} = (z_0/\tilde{z})^{2n} n^{2-2\gamma} K_{bulk}$. To describe the surface reaction, we utilize $\tilde{Z}_p = \tilde{z}^n n^{\gamma_s-1}$ with $\gamma_s = 0.695$ and $\tilde{Z}_{pt} = \beta z_0^{2n} K_{bulk}$ yielding $\tilde{K}_{pt} = \beta(z_0/\tilde{z})^{2n} n^{2-\gamma-\gamma_s} K_{bulk}$. The ratio $\tilde{K}_{pt}/\tilde{K}_{bulk} = \beta n^{\gamma-\gamma_s} \approx \beta n^{0.472}$ is close to $\beta n^{1/2}$ as obtained for the RW case.

The preceding discussion applies in the polymeric limit as discussed in the Introduction, i.e., $N_s/p_s > 1$ and $N_s/p_s + n/p_p \gg 1$. It reflects the effects of the impenetrable surface on the number of configurations available to freely jointed chains but does not allow for steric strain effects. In particular, it cannot describe the short spacer regime where $N_s/p_s \leq 1$, and the spacer effect may be traceable to the relief of steric strain. The experiments of Shchepinov et al.[15] and Guo et al.[16] suggest that K_{spt} increases with N_s in the range $0 \leq N_s/p_s \leq 1$ for both $N_t = n$ and $N_t \gg n$. This implies that the "local" steric effects decrease when the spacer length increases in the range $0 \leq N_s/p_s \leq 1$. The weakening of the local steric effect saturates for longer spacers when the polymeric approach is applicable. Combining this qualitative picture with the asymptotic trends eq 7 suggests that K_{spt} will exhibit a maximum in the range $0 \leq N_s/p_s \leq 2$ when $N_t = n$ (Figure 2 inset). In marked contrast, K_{spt} for $N_t \gg n$ will exhibit monotonic increase in this range. This provides a possible explanation for the results of Shchepinov et al.[15] on the effect of spacers when $n = N_t$ and reconciles it with the observations that, for long targets, the spacer benefits grow with N_t.

IV. Brush of Long Spacers with Short Probes

Different types of brushes can be formed at the probe layer of DNA oligonucleotide arrays depending on the relative magnitude of N_s, N_t, and n. A polyelectrolyte brush of ssDNA "tails" can be formed when $N_t \gg n \approx N_s$.[10,43] A mixed polyelectrolyte brush of rodlike hybridized probes and nonhybridized ss ones can develop when $N_t = n \gg N_s$.[9] In these two cases, considered previously, the role of the spacers is relatively

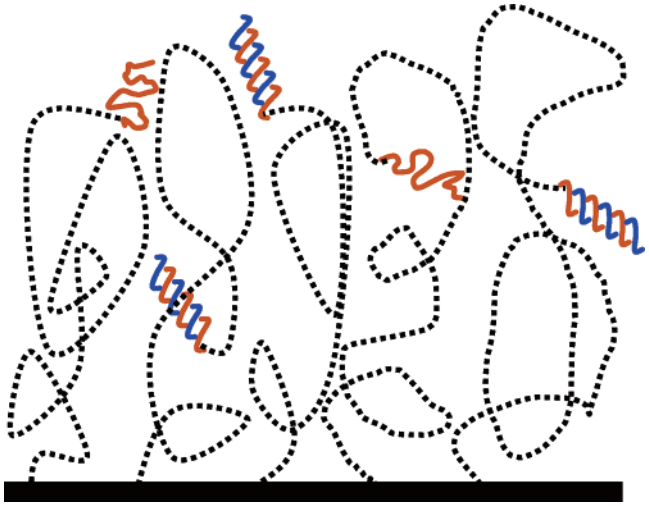

Figure 3. Brush of long flexible and neutral spacers carrying short probes that hybridize to targets of equal length.

minor. A case where the spacers play a key role occurs when $N_s \gg n = N_t \gg 1$ (Figure 3). In the following, we focus on this situation, when the sp and spt chains can be viewed as flexible neutral chains carrying terminal point charges corresponding to p and pt. The overlap threshold for the formation of such brush is determined by the length of the spacers. In a good solvent for the spacers, the onset of the brush regime occurs at $\Sigma \approx R_F^2$ where the Flory radius of the spacer is $R_F \approx N_s^{3/5} a_s$. In this section, we derive the leading structural characteristics of this brush and the corresponding hybridization isotherm as obtained from an Alexander type model.[12,14] In particular, we assume a steplike monomer concentration profile and uniformly stretched chains with their free ends straddling the upper boundary of the brush at height H. The corresponding free energy per probe site comprises four terms, $\gamma_{site} = F_{el} + F_{int} + F_{mix} + F_{hyb}$. The first is the Gaussian elastic free energy of a spacer chain stretched from $R_0 \simeq N_s^{1/2} a_s$ to H or $F_{el} \simeq kTH^2/R_0^2$. The second term, F_{int}, allows for the different types of monomer−monomer interactions. It comprises, thus, three terms, reflecting spacer−spacer, probe−probe, and spacer−probe interactions, denoted, respectively, by F_s, F_p, and F_{sp}. $F_s = kT\upsilon_s c_s^2 V_{chain}$ where $c_s = N_s/V_{chain}$ is the concentration of spacer monomers, $V_{chain} = \Sigma H$ is the volume per chain, and $\upsilon_s \approx a_s^3(1 - \theta_s/T)$ is the corresponding virial coefficient. Here, a_s and θ_s denote the spacer monomer size and the theta temperature of the spacer, respectively. We utilize similar expressions for F_p and F_{sp}. Thus, $F_p = kT\upsilon_p c_p^2 V_{chain}$, where the concentration of nucleotide bases $c_p = n(1 + x)/H\Sigma$ reflects, in the spirit of the Flory approximation, the contribution arising from both ss and ds probes. In other words, the interactions between the probes, hybridized or not, are approximated by the binary interactions in the corresponding solution of disconnected bases. Since the nucleotide bases are charged, $\upsilon_p \approx a_p^3(1 - \theta_p/T) + l_B r_D^2$ where a_p is a typical base size and θ_p is its theta temperature. The term allowing for spacer−probe interactions is $F_{sp} = kT\upsilon_{sp} c_s c_p V_{chain}$ where we will assume that $\upsilon_{sp} \approx \upsilon_s$. The mixing entropy associated with the different possible placements of sp and spt gives rise to $F_{mix}/kT = x \ln x + (1 - x) \ln(1 - x)$. Finally, $F_{hyb} = x\mu_{pt}^0 + (1 - x)\mu_p^0$ reflects the free energy gain due to the hybridization of the probes. μ_{pt}^0 and μ_p^0 are the standard chemical potentials of the hybridized and nonhybridized probes. Altogether,

(43) Halperin, A.; Buhot, A.; Zhulina, E. B. *J. Phys.: Condens. Matter* **2006**, *18,* S463−S490.

$$\frac{\gamma_{site}}{kT} \simeq \frac{H^2}{N_s a_s^2} + \frac{1}{H\Sigma}[\upsilon_s N_s^2 + \upsilon_p n^2(1+x)^2 + \upsilon_{sp} N_s n(1+x)] + x\ln x + (1-x)\ln(1-x) + x\frac{\mu_{pt}^0}{kT} + (1-x)\frac{\mu_p^0}{kT} \quad (21)$$

where we have omitted numerical prefactors of order unity. Notice that the interaction term does not allow for the localization of the probe monomers at the free end restricted to altitude H. It is indistinguishable from that of a random copolymer. The use of this interaction free energy is nevertheless justified because the probes are actually distributed throughout the brush, as will be discussed in the next section. In the following, γ_{site} does not reflect the effect of the impenetrable wall because it diminishes with the extension of the chains and is, thus, negligible for dense brushes.[10]

The equilibrium condition for a given x as given by $\partial\gamma_{site}/\partial H = 0$ is

$$\frac{H_{eq}}{H_0} \simeq \left[1 + \frac{\upsilon_p}{\upsilon_s}\left(\frac{n}{N_s}\right)^2(1+x)^2 + \frac{\upsilon_{sp}}{\upsilon_s}\frac{n}{N_s}(1+x)\right]^{1/3} \quad (22)$$

where

$$H_0 \simeq \upsilon_s^{1/3} N_s (a_s^2/\Sigma)^{1/3} \quad (23)$$

is the height of a "pure spacer" brush. In equilibrium, the elastic free energy is comparable to the total interaction free energy, thus yielding H_{eq}. The equilibrium free energy per site, as obtained from substituting H_{eq} into γ_{site}, is

$$\frac{\gamma_{site}}{kT} \simeq N_s\left(\frac{\upsilon_s}{a_s\Sigma}\right)^{2/3}\left[1 + \frac{\upsilon_p}{\upsilon_s}\left(\frac{n}{N_s}\right)^2(1+x)^2 + \frac{\upsilon_{sp}}{\upsilon_s}\frac{n}{N_s}(1+x)\right]^{2/3} + x\ln x + (1-x)\ln(1-x) + x\frac{\mu_{pt}^0}{kT} + (1-x)\frac{\mu_p^0}{kT} \quad (24)$$

The hybridization isotherm is determined by the equilibrium condition $\partial\gamma_{site}/\partial x = \mu_t^0 + kT\ln c_t$, thus leading to

$$\frac{x_{eq}}{1-x_{eq}} = c_t K_{bulk}\exp[-\Gamma(x_{eq})] \quad (25)$$

where

$$K_{bulk} = \exp\left[-\frac{\mu_{pt}^0 - \mu_p^0 - \mu_t^0}{kT}\right] \quad (26)$$

and

$$\Gamma(x_{eq}) \simeq n\left(\frac{\upsilon_s}{a_s\Sigma}\right)^{2/3}\frac{\frac{\upsilon_p}{\upsilon_s}\frac{n}{N_s}(1+x) + \frac{\upsilon_{sp}}{\upsilon_s}}{\left[1 + \frac{\upsilon_p}{\upsilon_s}\left(\frac{n}{N_s}\right)^2(1+x)^2 + \frac{\upsilon_{sp}}{\upsilon_s}\frac{n}{N_s}(1+x)\right]^{1/3}} \quad (27)$$

When $n \ll N_s$ and $\upsilon_{sp} \approx \upsilon_s$, the third term in the square brackets is negligible, $(\upsilon_{sp}/\upsilon_s)(n/N_s)(1+x) \ll 1$. We can thus distinguish between three regimes. The first is specified by $N_s/n(1+x) < \sqrt{\upsilon_p/\upsilon_s} < \upsilon_p/\upsilon_s$ or $F_p > F_s > F_{sp}$. In other words, the probe−probe interaction dominates. In this probe-dominated regime,

$$H_{eq} \simeq \upsilon_p^{1/3} N_s^{1/3} n^{2/3}(a_s^2/\Sigma)^{2/3}(1+x_{eq})^{2/3} = H_0[n(1+x_{eq})/N_s]^{2/3} \quad (28)$$

$$\Gamma(x_{eq}) \simeq \frac{n^{4/3}}{N_s^{1/3}}\left(\frac{\upsilon_p}{a_s\Sigma}\right)^{2/3}(1+x_{eq})^{1/3} \quad (29)$$

$$c_{50} \simeq \frac{1}{K_{bulk}}\exp\left[\frac{n^{4/3}}{N_s^{1/3}}\left(\frac{\upsilon_p}{a_s\Sigma}\right)^{2/3}\right] \quad (30)$$

where c_{50} is the target concentration for which 50% of the probes are hybridized. This regime reflects a balance between the electrostatic repulsion among the charged terminal groups and the Gaussian elasticity of the spacers. It was considered earlier, without the effect of hybridization reaction, in ref 44. In distinction to "normal" brushes, the interactions between the spacer monomers do not contribute to the swelling of the brush. Importantly, in this regime, the brush thickness varies with x_{eq} and, thus, with c_t. H_{eq} grows by ~60% as x_{eq} approaches unity, that is, as the target concentration increases from zero to $c_t \gg c_{50}$.

In contrast, when $\sqrt{\upsilon_p/\upsilon_s} < N_s/n(1+x)$, or $F_s > F_p$, the equilibrium height $H_{eq} \approx H_0$ reflects an interplay between the spacers' monomer−monomer interactions and their Gaussian elasticity and there is no dependence of H_{eq} on x_{eq}. Within this spacer-dominated regime, it is possible to distinguish two subregimes characterized by different $\Gamma(x_{eq})$. In particular, for $\sqrt{\upsilon_p/\upsilon_s} < N_s/n(1+x) < \upsilon_p/\upsilon_s$ or $F_s > F_p > F_{sp}$, the hybridization is opposed by the electrostatic penalty incured upon inserting the targets into the probe layer, thus leading to

$$\Gamma(x_{eq}) \simeq \frac{\upsilon_p}{\upsilon_s}\frac{n^2}{N_s}\left(\frac{\upsilon_s}{a_s\Sigma}\right)^{2/3}(1+x_{eq}) \quad (31)$$

and

$$c_{50} \simeq \frac{1}{K_{bulk}}\exp\left[\frac{\upsilon_p}{\upsilon_s}\frac{n^2}{N_s}\left(\frac{\upsilon_s}{a_s\Sigma}\right)^{2/3}\right] \quad (32)$$

In contrast, these interactions are negligible when $\sqrt{\upsilon_p/\upsilon_s} < \upsilon_p/\upsilon_s < N_s/n(1+x)$ or $F_s > F_{sp} > F_p$. In this last regime, the hybridization is opposed by the interactions between the spacer and target monomers. As a result,

$$\Gamma(x_{eq}) \simeq n\left(\frac{\upsilon_s}{a_s\Sigma}\right)^{2/3} \quad (33)$$

is independent of x_{eq} and

$$c_{50} \simeq \frac{1}{K_{bulk}}\exp\left[n\left(\frac{\upsilon_s}{a_s\Sigma}\right)^{2/3}\right] \quad (34)$$

Overall, $\Gamma(x_{eq})$ decreases as N_s/n increases, essentially attaining its saturation value when $N_s = N_s^{sat} = n\upsilon_p/\upsilon_s > n$. To quantify the spacer benefits in the brush regime, it is useful to compare two effective equilibrium constants. One,

$$K_{spt}^{brush}(N_s) \simeq K_{bulk}\exp\left[-n\left(\frac{\upsilon_s}{a_s\Sigma}\right)^{2/3}\right] \quad (35)$$

(44) Birshtein, T. M.; Zhulina, E. B.; Pryamitsyn, V. A. *Polym. Sci., Ser. A* **1997**, *37*, 1186−1192.

describes the best possible spacer performance, as attained upon saturation of the beneficial effect of the increased spacer length. The second, K_{pt}^{brush}, describes the hybridization at the brush regime with no spacers.[9] In this last case, the brush is formed because of an overlap between the probes attached to the surface via flexible short linkers that enable hybridization and free rotation but do not contribute to the H_{eq}. K_{pt}^{brush} for $N_t = n$ and short probes with $10 \le n \le 20$ is

$$K_{pt}^{brush} = K_{bulk} \exp[-\Gamma_0(1 + x_{eq})] \quad (36)$$

where $\Gamma_0 \approx \upsilon_p n/b\Sigma$.[9] The ratio

$$\frac{K_{spt}^{brush}(N_s)}{K_{pt}^{brush}} \simeq \exp\left\{ n\left[\frac{\upsilon_p}{b\Sigma}(1 + x_{eq}) - \left(\frac{\upsilon_s}{a_s\Sigma}\right)^{2/3}\right]\right\} \quad (37)$$

exceeds unity at high grafting densities when the area per chain is lower than $\Sigma_{co} = \upsilon_p^3 a_s^2/\upsilon_s^2 b^3$. In physical terms, Σ_{co} corresponds to $F_p(N_s = 1) = F_{sp}(N_s \gg n)$. When $\Sigma > \Sigma_{co}$, longer spacers afford no benefit in the brush regime because the spacer−probe interactions are negligible. On the other hand, when $\Sigma < \Sigma_{co}$, it is useful to increase N_s up to its saturation value N_s^{sat} in order to lower this penalty.

As expected, utilization of polyanion spacers, such as oligonucleotides, diminishes the spacer benefits in the brush regime. Within our approach, the interaction free energy in this case is $F_{int} = kT\upsilon_p[N_s + n(1 + x)]^2/H\Sigma$. When $N_s \gg n$, the equilibrium height of the brush is $H_{eq} \approx N_s(\upsilon_p a_p^2/\Sigma)^{1/3}$ and $\Gamma(x_{eq}) \approx n(\upsilon_p/a_p\Sigma)^{2/3}$. Comparison to the short linker case reveals that spacer benefits occur at much higher grafting densities, when $\Sigma < \Sigma_{co} \approx \upsilon_p a_p^2/b^3$ as compared to $\Sigma_{co} \approx \upsilon_p^3 a_s^2/\upsilon_s^2 b^3$ in the case of neutral spacers in an athermal solvent. Note that the charge density of the copolymer spacers utilized by Shchepinov et al.[15] is intermediate with respect to the two cases considered above.

V. Brush of Long Spacers with Short Probes: SCF Theory

The simplicity of the Alexander type model utilized in the previous section is achieved at a price. The concentration profiles of the monomers and of the free ends are assumed rather than derived. The model overconstrains the system by assuming a steplike monomer concentration profile and localizing all free ends at the edge of the brush. To obtain the correct monomer and end-point concentration profiles, it is necessary to formulate the appropriate self-consistent field (SCF) theory. A full SCF theory, covering all the regimes considered, is beyond the scope of this article. It is, however, useful to consider the easily accessible SCF scenarios. The motivation is 3-fold. First, it is of importance to establish the robustness of the Alexander type approach. Two issues are involved. One concerns reliablity of the model for the probe-dominated regime, i.e., $N_s \gg N_t = n$, and solutions of intermediate ionic strength. The performance of the Alexander model in this regime has not been studied thus far, and it is useful to compare its results to those obtained via more rigorous techniques. This is in contrast to the spacer-dominated regime, where the brushes are essentially equivalent to the familiar homopolymer brushes and the performance of the Alexander model was confirmed by comparison with the SCF theory, computer simulations, and experiments.[44−48] The second point concerns the treatment of the hybridization equilibrium. Within the Alexander type model, the equilibrium fraction x_{eq} is uniform throughout the layer. The SCF theory allows one to characterize the height dependence of x. This is especially important in the probe-dominated regime where hybridization at the outer edge of the brush incurs a smaller interaction penalty. The final point concernes the SCF theory of the probe-dominated regime. As we shall see, it leads to distinctive monomer and end-point concentration profiles. This is of interest within the theory of polymer brushes because brushes of spacer−probe sp chains afford an opportunity to experimentally characterize the end-point distribution by selective labeling of the probes. Such experiments are much more difficult in brushes of homopolymers. It is helpful to first summarize the formulation of the SCF theory for our model. We will then analyze the experimentally accessible case of the nonhybridized brush with $x = 0$. The height dependence of the hybridization degree will be considered last.

The free energy per probe site comprises the four contributions discussed in the previous section, $\gamma_{site} = F_{el} + F_{int} + F_{mix} + F_{hyb}$. The elastic free energy assumes the familiar form, as obtained for normal brushes,[45−47] that is,

$$F_{el} = \frac{3kT}{2a_s^2}\int_0^H \mathrm{d}h g(h)\int_0^h E(z, h)\,\mathrm{d}z. \quad (38)$$

Here $E(z, h) = \mathrm{d}z/\mathrm{d}N_s$ is proportional to the local tension, $3kTE(z, h)/a_s^2$ at altitude z, in a spacer chain whose free end is localized at height h, and $g(h)$ is the fraction of free ends per unit length situated at h. The concentration profile of spacer monomers is specified by

$$c_s(z) = \frac{1}{\Sigma}\int_z^H \frac{g(h)}{E(z, h)}\,\mathrm{d}h \quad (39)$$

The interaction free energy

$$F_{int} = F_p + F_s + F_{sp} = kT\Sigma\int_0^H [\upsilon_p c_p^2(z) + \upsilon_s c_s^2(z) + 2\upsilon_{sp} c_s(z) c_p(z)]\,\mathrm{d}z \quad (40)$$

reflects the three types of binary interactions in a good solvent as discussed previously. The laterally uniform concentration profile of the probe and target bases is specified by $c_p(z) = n[1 + x(z)]g(z)/\Sigma$ where $x(z)$ is the hybridization fraction at z. The terms discussed until now play a role for nonhybridized as well as for hybridized brushes. To describe the hybridization behavior, it is necessary to allow for the mixing entropy of p and pt and the hybridization energy of the probes. The SCF counterparts of F_{mix} and F_{hyb} are

$$F_{mix} = kT\int_0^H g(z)\{x(z)\ln x(z) + [1 - x(z)]\ln[1 - x(z)]\}\,\mathrm{d}z \quad (41)$$

$$F_{hyb} = \int_0^H g(z)\{x(z)\mu_{pt}^0 + [1 - x(z)]\mu_p^0\}\,\mathrm{d}z \quad (42)$$

For future convenience, it is helpful to replace F_{hyb} by

$$\Delta F_{hyb} = \int_0^H g(z)\{x(z)\mu_{pt}^0 + [1 - x(z)]\mu_p^0 - x(z)[\mu_t^0 + kT\ln c_t]\}\,\mathrm{d}z \quad (43)$$

allowing for the total change of free energy upon hybridization. The equilibrium condition is then specified by minimization of

(45) Semenov, A. N. *Sov. Phys. JETP* **1985**, *61*, 733.
(46) Zhulina, E. B., Borisov, O. V.; Priamitsyn, V. A. *Polym. Sci. U.S.S.R.* **1989**, *31*, 205−216.
(47) Milner, S. T.; Witten, T. A.; Cates, M. E. *Macromolecules* **1988**, *21*, 2610−2619.
(48) Grest, G. S.; Murat, M. *Macromolecules* **1993**, *26*, 3108−3117.

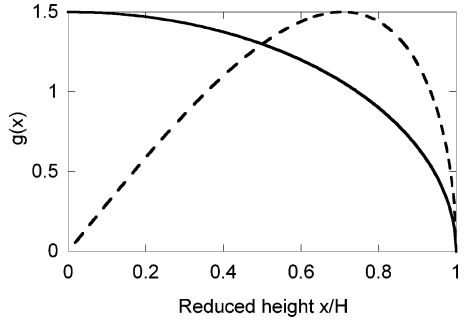

Figure 4. Plot of $g(z)$ vs z for the probe-dominated brush (—) as compared to a normal brush (- - -).

γ_{site} with respect to $x(z)$ instead of $\partial\gamma_{site}/\partial x = \mu_t^0 + kT \ln c_t$ as before. The brush structure is determined by minimization of γ_{site} with respect to $E(z, h)$, $g(h)$, and $x(z)$ subject to two constraints. One is that each spacer consists of N_s monomers

$$\int_0^h \frac{dz}{E(z, h)} = \int_0^h dN_s(z) = N_s \tag{44}$$

and the second is the normalization condition

$$\int_0^H g(z)\, dz = 1 \tag{45}$$

The brush thickness H is determined by the requirement that $c_s(H) = c_p(H) = 0$.

Our subsequent analysis concerns two regimes. One, the spacer-dominated regime, is characterized by $F_{int} \approx F_s$ or $F_{sp} \approx F_p \ll F_s$ in the notation of the previous section. In the second, probe-dominated regime, $F_{int} \approx F_p$, that is, $F_{sp} \approx F_s \ll F_p$. We first discuss the nonhybridized brush case, $x = 0$. For comparison purposes and future reference, we list side by side the leading brush characteristics for the two cases. As noted before, the spacer-dominated regime reduces to the case of the familar homopolymer brush. The brush characteristics corresponding to this case will be denoted by the index 0, for example, H_0 for its equilibrium height, etc. The brush structure for the probe or free-end-dominated case is obtained in Appendix B. The characteristics corresponding to this case will be denoted by the index e. An important difference between the two cases concerns the chain stretching. In the probe-dominated regime, the chains are uniformely stretched while their extension varies with z in the spacer-dominated regime

$$E_0(z, h) = \frac{\pi}{2N_s}\sqrt{h^2 - z^2} \quad \text{and } E_e(z, h) = \frac{h}{N_s} \tag{46}$$

The corresponding distibutions of ends are also different with a markedly dissimilar behavior in the vicinity of the surface (Figure 4),

$$g_0(z) = \frac{3z}{H_0^2}\sqrt{1 - \frac{z^2}{H_0^2}} \quad \text{and } g_e(z) = \frac{3}{2H_e}\left(1 - \frac{z^2}{H_e^2}\right) \tag{47}$$

As a result, the probe base concentration profiles in the two cases are dissimilar,

$$c_p^0(z) = \frac{3nz}{\Sigma H_0^2}\sqrt{1 - \frac{z^2}{H_0^2}} \quad \text{and } c_p^e(z) = \frac{3n}{2\Sigma H_e}\left(1 - \frac{z^2}{H_e^2}\right) \tag{48}$$

Importantly, the scaling form of the equilibrium free energy and the brush height as obtained by the SCF theory agrees with the

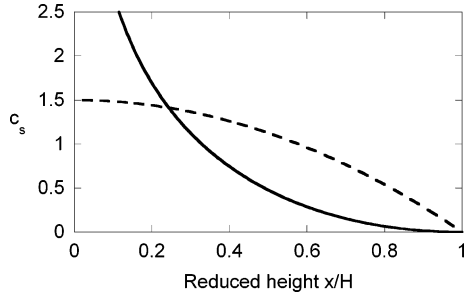

Figure 5. Plot of $c_s(z)$ vs z for the probe-dominated brush (—) as compared to a normal brush (- - -).

Alexander type analysis presented earlier,

$$\frac{F_0}{kT} = \frac{9}{10}N_s\left(\pi\upsilon_s\frac{a_s^2}{\Sigma}\right)^{2/3} \quad \text{and } \frac{F_e}{kT} = \frac{9}{10}N_s\left(2\upsilon_p\frac{n^2a_s^2}{N_s^2\Sigma}\right)^{2/3} \tag{49}$$

$$H_0 = \left(\frac{8}{\pi}\right)^{1/3} N_s\left(\upsilon_s\frac{a_s^2}{\Sigma}\right)^{1/3} \quad \text{and } H_e = \left(2N_sn^2\upsilon_p\frac{a_s^2}{\Sigma}\right)^{1/3} \tag{50}$$

The concentration profiles of spacer monomers in the two cases are markedly different,

$$c_s^0(z) = \frac{3N_s}{\Sigma H_0}\left(1 - \frac{z^2}{H_0^2}\right)$$

$$\text{and } c_s^e(z) = \frac{3}{2\Sigma H_e}\frac{N_s}{}\left[\ln\left(\frac{H_e}{z}\right) - \frac{1}{2}\left(1 - \frac{z^2}{H_e^2}\right)\right] \tag{51}$$

The concentration profile $c_s^e(z)$ in eq 51 exhibits an unphysical logarithmic divergence at the origin (Figure 5). It is traceable to the range of validity of the underlying assumption that $c_s^e(z)\sqrt{\upsilon_s} \ll c_p^e(z)\sqrt{\upsilon_p}$. Equations 48 and 51 lead to

$$\frac{c_s^e(z)\sqrt{\upsilon_s}}{c_p^e(z)\sqrt{\upsilon_p}} = \sqrt{\left(\frac{N_s}{n}\right)^2\frac{\upsilon_s}{\upsilon_p}}\left[\left(1 - \frac{z^2}{H_e^2}\right)^{-1}\ln\left(\frac{H_e}{z}\right) - \frac{1}{2}\right] \tag{52}$$

In the regime considered, $N_s/n < \sqrt{\upsilon_p/\upsilon_s}$, ensuring that the square root factor is always smaller than unity. The second factor is of order unity when $z/H_e \approx 0.2$ and is larger for $z/H_e < 0.2$. The logarithmic divergence of $c_s^e(z)$ near the surface creates a region with $c_s^e(z)/c_p^e(z) > 1$, and the underlying assumption is not satisfied. This assumption is, however, satisfied in most of the brush, and our results provide a reasonable description for the concentration profiles of the monomers and the free ends in the $z/H_e > 0.2$ region.

With this in mind, we turn to the hybridization behavior within the SCF theory. The spacer-dominated case, when p and sp interactions are negligible, is straightforward. By definition, the brush structure is weakly affected by the hybridization fraction. When $F_p = F_{sp} = 0$, the brush is characterized by $g(z) = g_0(z)$ and $c_s(z) = c_s^0(z)$. The hybridization isotherm at z, as determined by minimizing $\gamma_{site} = F_0 + F_{mix} + \Delta F_{hyb}$ with respect to $x(z)$, leads to $x(z) = x_{bulk}$ as specified by the bulk Langmuir isotherm,

$$\frac{x_{bulk}}{1 - x_{bulk}} = c_tK_{bulk} \tag{53}$$

The corresponding concentration profile of p and pt bases is $c_p^0(z) = n(1 + x_{bulk})g_0(z)/\Sigma$. This result is not surprising because there is no extra hybridization penalty due to p and sp interactions. When probe−probe and spacer−probe interactions do play a

role, the hybridization fraction does vary with z (Appendices C and D). In these situations, the hybridization at the outer edge of the brush is favored. It is instructive to consider this effect in two limits, when the p and sp interactions give rise to first-order corrections to F_0. Clearly, in both cases, $x(z) < x_{bulk}$. When the p interactions are weaker than the sp ones, $F_p < F_{sp}$,

$$\frac{x(z)}{1-x(z)} = c_t K_{bulk} \exp[-\upsilon_{sp} n c_s^0(z)] \tag{54}$$

and the z-dependence of the exponent is due to the parabolic behavior of $c_s^0(z)$. As a result, $x(z)$ decreases monotonically from $x(z = H_0) = x_{bulk}$ and attains its minimal value $x(z = 0) = x_0$ at the surface. In the opposite case of $F_p > F_{sp}$,

$$\frac{x(z)}{1-x(z)} = c_t K_{bulk} \exp\left\{-\frac{2\upsilon_p n^2}{\Sigma}[1+x(z)]g_0(z)\right\} \tag{55}$$

and the z-dependence of the exponent is nonmonotonic: $g_0(z)$ exhibits a maximum and $x(z)$ exhibits a corresponding minimum in the interior of the brush. In this case, $x(z = H_0) = x(z = 0) = x_{bulk}$. In both limits, the average hybridization degree within the brush

$$x_{av} = \int_0^{H_0} g_0(z)x(z)\,dz < x_{bulk} \tag{56}$$

is lower than in the bulk because of the p and sp interactions (Appendix D). The z-dependent hybridization isotherms, eqs 54 and 55, are the SCF counterparts of the corresponding isotherms in Section IV. Importantly, the prefactors before the z-dependent functions in the exponents agree with the corresponding expressions for Γ in eqs 33 and 31 of the previous section, thus supporting the results of the Alexander type approach.

The SCF description of the probe-dominated regime can be simplified because the elastic free energy of uniformly stretched chains is

$$F_{el} = \frac{3kT}{2N_s a_s^2}\int_0^H g(z)z^2\,dz \tag{57}$$

In this limit, probe−probe interactions dominate and $F_{int} \approx F_p$ with

$$\frac{F_p}{kT} = \frac{\upsilon_p n^2}{\Sigma}\int_0^H g^2(z)[1+x(z)]^2\,dz \tag{58}$$

Within this approximation, the bases of the p and pt at altitude z are uniformly distributed laterally. This $F_{int} \approx F_p$ case is qualitatively different from the familiar $F_{int} \approx F_s$, describing a normal brush which allows for the interactions between all the spacer monomers rather than singling out the interactions between the free ends. Note that the two unknown functions $g(z)$ and $x(z)$ are now coupled in F_p. The $F_p > F_s > F_{sp}$ regime, where the probe−probe interactions dominate, is associated with a novel hybridization isotherm as discussed in Section IV and Appendix C. At intermediate hybridization degrees, $0 < x_{av} < 1$, the hybridization fraction varies with the altitude as

$$\frac{x(z)}{1-x(z)} = c_t K_{bulk}\left[\frac{1-x(z)}{1-x_{bulk}}\right]\exp\left\{-\frac{3[H_e^2(x_{av}) - z^2]}{2N_s a_s^2}\right\} \tag{59}$$

where the brush thickness $H_e(x_{av})$ is determined from the normalization condition eq 45 with

$$g(z) = -\frac{\Sigma}{2\upsilon_p n^2[1+x(z)]}\ln\left\{\frac{x(z)(1-x_{bulk})}{[1-x(z)]x_{bulk}}\right\} \tag{60}$$

Clearly, the hybridization at the outer edge of the brush is favored because it does not incur an interaction penalty. Simple analytical results are possible in the two limits of $x(z) \ll 1$ and $x(z) \approx 1$ (Appendix D). The hybridization isotherm eq 59 differs from the one obtained using the Alexander type approach, eq 29, in the fact that x is z-dependent. It is, thus, a local rather than global isotherm. It also differs in having an extra $[1 - x(z)]/[1 - x_{bulk}]$ factor. On the other hand, the combination of parameters in the exponent

$$\frac{H_e^2}{N_s a_s^2} \simeq \frac{n^{4/3}}{N_s^{1/3}}\left(\frac{\upsilon_p}{a_s\Sigma}\right)^{2/3} \tag{61}$$

matches the corresponding expression for Γ in eq 29, thus lending support to our earlier, simplified, analysis.

The relative weights of the different regimes vary with the salt concentration, c_{salt}. Increasing c_{salt} leads to a corresponding decrease in r_D and υ_p. In turn, the spacer-dominated regime gains in importance and its SCF description becomes asymptotically rigorous when $N_s/n \to \infty$.

VI. Discussion

As noted in the Introduction, the general agreement on the positive role of spacers was somewhat impaired by diverging reports on the range of parameters leading to beneficial effects. Our discussion suggests that the diverging results are traceable to different experimental conditions. Two issues are of special importance. First, different behavior is expected for short targets, $N_t = n$, and for long targets, $N_t \gg n$. Second, brush effects come into play at high surface densities. Our analysis focused on the effect of the spacer length N_s on equilibrium state of the hybridization reaction as characterized by the hybridization isotherms. In particular, it concerned the effect of spacers on the hybridization equilibrium at the surface. When the surface density of the probes is low, the dominant effect is due to the impenetrable surface. This reduces the number of accessible chain trajectories of terminally anchored mushrooms, thus affecting the entropy of the reactants and the products. Spacers weaken the surface effect and the hybridization behavior approaches its bulk characteristics when the spacers are very long. However, the effect depends strongly on the target length. For long targets, spacers improve the hybridization. In contrast, the asymptotic behavior of long spacers in the case of short targets suggests a detrimental effect. Yet, in combination with a fast decaying beneficial effect in relieving the steric strain at the grafting site, it suggests a nonmonotonic effect of the spacer length when the targets are short. At high grafting densities, the chains at the probe layer crowd each other, thus giving rise to a polymer brush. Different types of brushes are possible, depending on n, N_s, and N_t. Our analysis focused on a distinctive brush regime where the spacer chains play a key role, in particular, the case of long spacers carrying short probes hybridizing to targets of identical length. At intermediate ionic strength, the stretching elasticity of the spacers is balanced by the electrostatic interactions between the probes.

Hybridization reactions at a surface are analogous to the adsorption process, as is evident from the utility of the Langmuir isotherm in the analysis. It is, however, important to note the distinctive features of the hybridization onto a DNA chip as compared to adsorption onto an unfunctionalized solid surface.

First, the bulk hybridization of free probes and targets provides a well-characterized reference, allowing one to identify surface effects. Second, it is possible to tune the density of the adsorption sites as well as the adsorption free energy. These two features also characterize analytical techniques involving binding of ligands or antibodies to proteins immobilized at surfaces, for example, the Western blot. However, in such assays, the proteins are in a folded state and their configurational statistics play a negligible role. Moreover, the structure of the protein reactants is typically not a design option. In contrast, for DNA chips the configurational statistics of the chains do play a role. Furthermore, the probe sequence, Σ, n, and N_s as well as the target length, N_t, are experimentally controlled. Altogether, the polymeric character of the adsorbing species, the targets, and the adsorption sites, the probes, give rise to tuning parameters having no counterpart in other adsorption processes. Because of the points listed above, it is both possible and desirable to develop theoretical models for hybridization at the surface of DNA microarrays. In particular, a polymer physics approach allows us to analyze the effect of the configurational statistics of the reactants and the products on the hybridization behavior. It is useful to develop such theoretical models in order to obtain compact guidelines concerning the multitude of design parameters involved.

As noted previously, the experimental studies of spacer effects utilized stepwise addition of monomers. This is clearly the strategy of choice for in situ synthesis. It is also advantageous when short oligonucleotide spacers are incorporated into presynthesized targets. However, this approach clearly limits the accessible range of spacer chains. Accordingly, physical chemistry experiments on the role of spacers may benefit from different synthetic approaches, involving conjugation of the probes to neutral chains, such as PEO, whose polymerization degrees vary over a significant range. This will allow one to systematically investigate the effects of the spacer length on the hybridizations isotherms as discussed above. In particular, it is of interest to test the hybridization behavior of both short and long targets. As we discussed, such experiments will help to shed light on the function of spacer chains in DNA chips. However, such experiments are also of fundamental interest from the points of view of polymer and surface science. First, the effect of the spacers on the hybridization constants K_{spt} provides a novel method for experimental characterization of the surface exponent γ_s. Second, brushes of long spacers carrying short probes may provide a possibility of labeling the free ends, thus allowing for experimental determination of their spatial distribution. This, together with the novel regimes expected in these systems, makes them of interest from the perspective of polymer brush research. Inasmuch as such experiments aim to characterize the equilibrium hybridization isotherms, it is important to bear in mind the possibility of very slow equilibration rates.[49,50]

Acknowledgment. E.B.Z. acknowledges financial support from the CEA-Grenoble as well as the Russian Foundation for Basic Research (Grant 05-03-33126).

Appendix A: Partition Functions of pt and spt Chains at the Surface

The discussion of the three partition functions obtained in this Appendix assumes that the flexible chain blocks exhibit random walk statistics with $p_s = p_p = 1$.

1. Long Target Hybridized to a Probe Anchored via Short, Freely Rotating Linker. Upon hybridization to a long target $N_t > n$, the probe turns into a rod−coil diblock. A rodlike dsDNA domain comprising n base pairs is attached to the surface, and it carries an ssDNA tail of $N_t - n$ bases. Assuming that the junction between the rodlike domain and the surface is flexible allows one to specify the height y of the rod−coil junction with respect to the surface in terms of Θ the angle between the rod and the surface. In particular, $y = bn \sin \Theta$, where bn is the length of the rod. Within this picture, the rod is free to rotate around the normal to the surface and the corresponding rotational partition function for a given y

$$Z_{rot}(y)\,dy = \beta Z_{rot}^{free} \cos(\Theta)\,d\Theta = \beta Z_{rot}^{free} \frac{dy}{bn} \qquad (A1)$$

satisfies $\int_0^{bn} Z_{rot}(y)\,dy = \beta Z_{rot}^{free}$. The placement of the rod−coil junction at height y weakens the effect of the surface on Z_{tail}, the partition function of the unhybridized tail. To account for the role of y, we utilize the following approximation

$$Z_{tail}(N_t - n, y) = \begin{cases} \frac{y}{a_p} Z_{mush}(N_t - n) & \text{for } y < R_0 \\ Z_{free}(N_t - n) & \text{for } y > R_0 \end{cases} \qquad (A2)$$

where $R_0 = a_p\sqrt{N_t - n}$ is the span of the tail considered as an ideal chain.[51−53] In other words, when R_0 is smaller than y, we assume that there is no surface effect on Z_{tail}. We can now specify the partition function of pt as

$$Z_{pt} = z_0^{2n} \exp\left(-\frac{\Delta\tilde{G}_{bulk}^0}{RT}\right) \int_0^{bn} Z_{rot}(y) Z_{tail}(N_t - n, y)\,dy \qquad (A3)$$

where $z_0^{2n} \exp(-\Delta\tilde{G}_{bulk}^0/RT) Z_{rot}(y)$ is the partition function of the dsDNA with its coil junction at height y. It differs from Z_{pt}(free) of a free dsDNA with $N_t = n$ base pairs in that Z_{rot}^{free} is replaced by a reduced $Z_{rot}(y)$.

For long targets, $N_t > n + (bn/a_p)^2$ or $R_0 > bn$,

$$\begin{aligned} Z_{pt} &= z_0^{2n} \exp\left(-\frac{\Delta\tilde{G}_{bulk}^0}{RT}\right) \beta Z_{rot}^{free} Z_{mush}(N_t - n) \int_0^{bn} \frac{y\,dy}{ba_p n} \\ &= z_0^{2n} \exp\left(-\frac{\Delta\tilde{G}_{bulk}^0}{RT}\right) \beta Z_{rot}^{free} \frac{Z_{free}(N_t - n)}{\sqrt{N_t - n}} \frac{bn}{2a_p} = \\ &\qquad \beta Z_{pt}(\text{free}) \frac{bn}{2R_0} \end{aligned} \qquad (A4)$$

where Z_{pt}(free) is the partition function for the free dsDNA with a free tail of $N_t - n \gg n$ bases. For short targets, $n \le N_t \le n + (bn/a_p)^2$ or $R_0 < bn$,

(49) Peterson, A. W.; Wolf, L. K.; Georgiadis, R. M. *J. Am. Chem. Soc.* **2002**, *124*, 14601−14607.
(50) Dai, H.; Meyer, M.; Stepaniants, S.; Ziman, M.; Soughton, R. *Nucleic Acids Res.* **2002**, *30*, e86.
(51) Chandrasekhar, S. *Rev. Mod. Phys.* **1943**, *15*, 1−89.
(52) DiMarzio, E. A. *J. Chem. Phys.* **1965**, *42*, 2101−2105.
(53) Feller, W. *An introduction to Probability Theory and its Applications*; John Wiley & Sons, Inc.: New York, 1968.

$$Z_{pt} = z_0^{2n} \exp\left(-\frac{\Delta\tilde{G}^0_{bulk}}{RT}\right)\beta Z^{free}_{rot}\left\{\int_0^{R_0} Z_{mush}(N_t - n)\frac{y\,dy}{ba_p n} + \int_{R_0}^{bn} Z_{free}(N_t - n)\frac{dy}{bn}\right\}$$

$$= z_0^{2n} \exp\left(-\frac{\Delta\tilde{G}^0_{bulk}}{RT}\right)\beta Z^{free}_{rot} Z_{free}(N_t - n)\left\{\frac{{R_0}^2}{2ba_p n\sqrt{N_t - n}} + \frac{bn - R_0}{bn}\right\} \quad \text{(A5)}$$

$$= \beta Z_{pt}(\text{free})\left(1 - \frac{R_0}{2bn}\right)$$

Substituting these expressions for Z_{pt} in eq 6 together with $Z_p = z_0^n n^{-1/2}$ leads to

$$\frac{K_{pt}}{K_{bulk}} = \begin{cases} \beta n^{1/2}\left(1 - \dfrac{a_p\sqrt{N_t - n}}{2bn}\right) & \text{for } n \le N_t \le n + (bn/a_p)^2 \\ \dfrac{\beta bn^{3/2}}{2a_p\sqrt{N_t - n}} & \text{for } N_t > n + (bn/a_p)^2 \end{cases} \quad \text{(A6)}$$

This ratio is a monotonically decreasing function of N_t, and the two branches merge at $N_t = n + (bn/a_p)^2$ or equivalently $bn = R_0 = a_p\sqrt{N_t - n}$.

2. Rodlike dsDNA with $n = N_t$ Tethered to a Surface via a Long Flexible Spacer. When a short rodlike ds pt is anchored to the surface via a flexible spacer chain, the corresponding partition function is

$$Z_{spt} = \int \beta(y) Z_{pt}(\text{free}) Z_{spacer}(y)\,dy = \beta_{av} Z_{pt}(\text{free}) Z_{spacer} \quad \text{(A7)}$$

Here, y is the position of the spacer−dsDNA junction. $\beta(y)$ is the reduction factor in the number of rotational configurations of a freely rotating rod with one end fixed at y with $\beta(y = 0) = \beta \approx 1/2$ and $\beta(y > bn) = 1$. $Z_{pt}(\text{free}) = z_0^{2n} \exp(-\Delta\tilde{G}^0_{bulk}/RT)\, Z^{free}_{rot}$, and $Z_{spacer}(y)$ is the partition function of a spacer chain with one end fixed at the surface and the other one at height y. The total partition function of the spacer allowing for all y is $Z_{spacer} = \int Z_{spacer}(y)\,dy = z_0 N_s N_s^{-1/2}$. The average value of $\beta(y)$ is $\beta_{av} = {Z_{spacer}}^{-1} \int \beta(y) Z_{spacer}(y)\,dy$.

3. Long Target Hybridized to a Short Probe Anchored to the Surface via a Long Flexible Spacer. The partition function of a coil−rod−coil triblock copolymer comprising a long ssDNA tail of length $N_t - n \gg 1$, a rigid dsDNA domain, and a flexible spacer grafted to the surface is

$$Z_{spt} = \int dy\, Z_{spacer}(y) \int_{y-bn}^{y+bn} dh\, Z_{pt}(n, y, h) Z_{tail}(N_t - n, h)$$
$$= \int dy\, Z_{spacer}(y) Z_{pt}(\text{free}) z_0^{n-N_t} Z_{tail}(N_t - n, y) \quad \text{(A8)}$$
$$= Z_{pt}(\text{free}) Z_{mush}(N_s + N_t - n) z_0^{n-N_t}$$

where y specifies the position of the spacer−dsDNA junction while h is the position of the dsDNA−ssDNA tail junction. $Z_{spacer}(y)$, $Z_{pt}(\text{free})$, and $Z_{tail}(N_t - n, h)$ are defined in the previous sections. The term $z_0^{n-N_t}$ compensates for the free ssDNA tail of $Z_{pt}(\text{free})$ lacking in $Z_{pt}(n, y, h)$. Here, we substituted $Z_{tail}(N_t - n, h)$ by $Z_{tail}(N_t - n, y)$ assuming that $bn \ll y$. Thus, from eq 6,

$$\frac{K_{spt}}{K_{bulk}} = \frac{Z_{mush}(N_s + N_t - n)}{z_0^{N_t - n}} \frac{Z_p(\text{free})}{Z_{sp}} = \left(\frac{N_s + n}{N_s + N_t - n}\right)^{1/2} \quad \text{(A9)}$$

Appendix B: SCF Theory of a Brush of Gaussian Chains with Terminally Charged Monomers

The equilibrium state of the brush is obtained from the minimization of $F_e = F_{el} + F_{int}$ with $F_{int} \approx F_p$,

$$\frac{F_e}{kT} = \int_0^H dh \left[\frac{3}{2{a_s}^2} g(h) \int_0^h E(z, h)\,dz + \frac{\upsilon_p n^2}{\Sigma} g^2(h) + \lambda_c(h) \int_0^h \frac{dz}{E(z, h)} + \lambda_n g(h)\right] \quad \text{(B1)}$$

where $\lambda_c(h)$ is the h-dependent Lagrange multiplier corresponding to constraint eq 44 while λ_n enforces the normalization condition eq 45. The variation of F_e with respect to $E(z, h)$ leads to $E_e(z, h) = 2{a_s}^2\lambda_c(h)/3g(h)$. In other words,

$$E_e(z, h) \equiv E(h) = h/N_s \quad \text{(B2)}$$

as determined by the conservation constraint eq 44, is independent of z in marked contrast to the normal brush case where $E_0(z, h) = \pi\sqrt{h^2 - z^2}/2N_s$. Substitution of $E(h)$ into eq B1 yields

$$\frac{F_e}{kT} = \int_0^H dh \left[\frac{3h^2}{2N_s{a_s}^2} g(h) + \frac{\upsilon_p n^2}{\Sigma} g^2(h) + \lambda_c(h) N_s + \lambda_n g(h)\right] \quad \text{(B3)}$$

Its variation with respect to $g(h)$ leads to $3h^2/2N_s{a_s}^2 + 2\upsilon_p n^2 g(h)/\Sigma + \lambda_n g(h) = 0$ or

$$g_e(z) = \frac{3\Sigma({H_e}^2 - z^2)}{4\upsilon_p n^2 N_s {a_s}^2} \quad \text{(B4)}$$

where we invoke the condition $c_p^e(z = H_e) = 0$ leading to $g_e(z = H_e) = 0$. This together with the normalization condition eq 45 yields $H_e = [2\upsilon_p N_s n^2 {a_s}^2/\Sigma]^{1/3}$, which, upon substitution in eq B4, determines $g_e(z)$.

Appendix C: SCF Theory of a Brush of Gaussian Chains with Terminally Charged Monomers—The Effect of Hybridization

The equilibrium hybridization of the brush is specified by the minimization of $\gamma_{site} = F_e + F_{mix} + \Delta F_{hyb}$ with respect to the two functions $g(z)$ and $x(z)$. F_e is given by eq B3 where n is replaced by $n[1 + x(z)]$ to account for the hybridized probes, thus leading to

$$\frac{\gamma_{site}}{kT} = \int_0^H \left\{\frac{3z^2}{2N_s{a_s}^2} g(z) + \frac{\upsilon_p n^2}{\Sigma} g^2(z)[1 + x(z)]^2 + \lambda g(z)\right\} dz + \int_0^H \{x(z) \ln x(z) + [1 - x(z)] \ln[1 - x(z)] - x(z) \ln(c_t K_{bulk})\} g(z)\,dz \quad \text{(C1)}$$

Here, λ is the Lagrange multiplier ensuring the normalization condition eq 45. The variation of γ_{site} with respect to $g(z)$ and $x(z)$ yields two equations

$$\frac{3z^2}{2N_s{a_s}^2} + \frac{2\upsilon_p n^2}{\Sigma} g(z)[1 + x(z)]^2 + \lambda + x(z) \ln \left(\frac{x(z)}{c_t K_{bulk}[1 - x(z)]}\right) + \ln[1 - x(z)] = 0 \quad \text{(C2)}$$

$$\frac{2\upsilon_p n^2}{\Sigma} g(z)^2[1 + x(z)] + g(z) \ln\left(\frac{x(z)}{c_t K_{bulk}[1 - x(z)]}\right) = 0 \quad \text{(C3)}$$

At the outer edge of the brush, $g(z = H) = 0$ and $x(z = H) = x_{bulk}$, leading to

$$\lambda = -\frac{3H^2}{2N_s{a_s}^2} - \ln(1 - x_{bulk}) \quad \text{(C4)}$$

This together with eqs C2 and C3 specifies the hybridization profile $x(z)$,

$$\frac{x(z)}{[1 - x(z)]^2} = \frac{x_{bulk}}{(1 - x_{bulk})^2} \exp\left[-\frac{3(H^2 - z^2)}{2N_s{a_s}^2}\right] \quad \text{(C5)}$$

and the distribution of the free ends, both p and pt,

$$g(z) = -\frac{\Sigma}{2\upsilon_p n^2[1 + x(z)]} \ln\left\{\frac{x(z)(1 - x_{bulk})}{[1 - x(z)]x_{bulk}}\right\} \quad \text{(C6)}$$

The equilibrium brush thickness H is obtained from the normalization condition eq 45. To determine the density profile $c_s(z)$ of spacer monomers, we use $E_e(z, h) = h/N_s$ (Appendix B), leading to

$$c_s(z) = \frac{1}{\Sigma}\int_z^H g(h) \frac{dN_s}{dh} dh = \frac{N_s}{\Sigma}\int_z^H \frac{g(h)}{h} dh \quad \text{(C7)}$$

Explicit analytical results can be obtained in the vicinity of $x_{bulk} = 0$ and $x_{bulk} = 1$. When $x_{bulk} \ll 1$ and, therefore, $x(z) \ll 1$, eqs C5 and C6 reduce to

$$\frac{x(z)}{x_{bulk}} = \exp\left[-\frac{3({H_e}^2 - z^2)}{2N_s{a_s}^2}\right] \quad \text{(C8)}$$

$$g_e(z) = -\frac{\Sigma}{2\upsilon_p n^2} \ln\left[\frac{x(z)}{x_{bulk}}\right] = \frac{3\Sigma({H_e}^2 - z^2)}{4\upsilon_p n^2 N_s{a_s}^2} \quad \text{(C9)}$$

The normalization condition eq 45 then yields the brush thickness

$$H_e(x_{bulk} \approx 0) = [2\upsilon_p N_s n^2 {a_s}^2/\Sigma]^{1/3} \quad \text{(C10)}$$

as well as $c_p^e(z) \approx n g_e(z)/\Sigma = 3n(1 - z^2/{H_e}^2)/2H_e\Sigma$. In this $x_{bulk} \ll 1$ limit, the average degree of hybridization in the brush is

$$x_{av} = \int_0^{H_e} g(z)x(z)\, dz = \frac{3x_{bulk}}{2}\int_0^1 \exp\left[-\frac{3{H_e}^2}{2N_s{a_s}^2}(1 - t^2)\right](1 - t^2)\, dt < x_{bulk} \quad \text{(C11)}$$

In the opposite limit of $1 - x_{bulk} \ll 1$ and $1 - x(z) \ll 1$, eq C5 reduces to

$$1 - x(z) = (1 - x_{bulk}) \exp\left[\frac{3({H_e}^2 - z^2)}{4N_s{a_s}^2}\right] \quad \text{(C12)}$$

while eq C6 becomes

$$g_e(z) = \frac{\Sigma}{4\upsilon_p n^2} \ln\left[\frac{1 - x(z)}{1 - x_{bulk}}\right] = \frac{3\Sigma({H_e}^2 - z^2)}{16\upsilon_p n^2 N_s{a_s}^2} \quad \text{(C13)}$$

Accordingly, $H_e(x_{bulk} \approx 1) = [8\upsilon_p N_s n^2 {a_s}^2/\Sigma]^{1/3}$ and $c_p^e(z) \approx 2n g_e(z)/\Sigma = 3n(1 - z^2/{H_e}^2)/H_e\Sigma$. In this $1 - x_{bulk} \ll 1$ limit, the average degree of hybridization in the brush satisfies

$$1 - x_{av} = \frac{3}{2}(1 - x_{bulk})\int_0^1 \exp\left[\frac{3{H_e}^2}{4{a_s}^2 N_s}(1 - t^2)\right](1 - t^2)\, dt > 1 - x_{bulk} \quad \text{(C14)}$$

thus $x_{av} < x_{bulk}$.

The hybridization clearly incurs a minimal penalty at the outer edge of the brush. Accordingly, the onset of hybridization, for $x_{bulk} \ll 1$, occurs at $z \le H_e$ and decays fast for lower z. As $x_{bulk} \to 1$, the hybridization penetrates into the depth of the brush but the innermost layer is the last to hybridize.

This refined analysis confirms the results of the scaling analysis concerning the increase of the brush height with hybridization. In particular, H_e increases by a factor of $4^{1/3} = 1.59$, when the hybridization degree grows from $x_{bulk} = 0$ to $x_{bulk} = 1$. The free end distributions c_p^e in these two limits exhibit the same functional form but differ in numerical factors because of the change in brush thickness H_e. Similarly, the concentration profile of spacer monomers in these two limiting cases is given by eq C7,

$$c_s^e(z) = \frac{3N_s}{2\Sigma H_e}\int_z^{H_e}\left(1 - \frac{h^2}{{H_e}^2}\right)\frac{dh}{h} = \frac{3N_s}{2\Sigma H_e}\left[\ln\left(\frac{H_e}{z}\right) - \frac{1}{2}\left(1 - \frac{z^2}{{H_e}^2}\right)\right] \quad \text{(C15)}$$

but the explicit form of $c_s^e(z)$ is different in the two limits because H_e varies with x_{bulk}.

Appendix D: SCF Theory of a "Normal" Brush with Noninteracting Probes—The Hybridization Profile for Very Long Spacers

In the case of long spacers and higher ionic strength, the interactions between the spacer monomers dominate the brush structure while the interactions involving the probes diminish in importance. In this scenario, where spacer−probe and probe−probe interactions are negligible, the hybridization degree is independent of the altitude, z. The total free energy per probe site is $\gamma_{site} = F_{el} + F_{int} + F_{mix} + \Delta F_{hyb} = F_0 + F_{mix} + \Delta F_{hyb}$, where F_0 as given by eq 49 is independent of $x(z)$. Thus, minimization with respect to $x(z)$ leads to a Langmuir isotherm,

$$\frac{x(z)}{1 - x(z)} = c_t K_{bulk} \quad \text{(D1)}$$

Accordingly, x is independent of z and $x(z) = x_{bulk}$. As noted above, this is in contrast to the z-dependent x found in Appendix C. The regime considered above is obtained so long as the interaction free energies with the probes are negligible compared to the interactions between the spacer monomers or $c_p^0(z)\sqrt{\upsilon_p} \ll c_s^0(z)\sqrt{\upsilon_s}$. In this regime, the laterally smeared concentration of bases, allowing for the hybridized probes, is

$$c_p^0(z) = \frac{n}{\Sigma}(1 + x_{bulk})g_0(z) = (1 + x_{bulk})\frac{3nz}{\Sigma {H_0}^2}\sqrt{1 - \frac{z^2}{{H_0}^2}} \quad \text{(D2)}$$

and the spacer concentration $c_s^0(z)$, eq 51, leads to

$$\frac{c_p^0(z)}{c_s^0(z)}\sqrt{\frac{\upsilon_p}{\upsilon_s}} = \frac{2n(1 + x_{bulk})}{N_s\sqrt{(1 - z^2/{H_0}^2)}}\frac{z}{H_0}\sqrt{\frac{\upsilon_p}{\upsilon_s}} \quad \text{(D3)}$$

This ratio is much smaller than unity when

$$\frac{z}{H_0} \ll \left\{1 + \left[\frac{N_s}{2n(1 + x_{bulk})}\right]^2\frac{\upsilon_s}{\upsilon_p}\right\}^{-1/2} \quad \text{(D4)}$$

Accordingly, the regime considered in this Appendix is realized in the major part of the brush in the limit of long spacers such that $N_s(\sqrt{\upsilon_s/\upsilon_p})/n(1 + x_{bulk}) \gg 1$.

It is possible to specify the first-order correction to the hybridization isotherm due to the probe interactions. When $F_{sp} > F_p$,

$$\gamma_{site} \approx F_0 + F_{sp} + F_{mix} + \Delta F_{hyb} = F_0 + kT\upsilon_{sp}n\int_0^{H_0}[1 + x(z)]g_0(z)c_s^0(z)\,dz + kT\int_0^{H_0} g_0(z)\{x(z)\ln x(z) + [1 - x(z)]\ln[1 - x(z)] - x(z)\ln(c_tK_{bulk})\}\,dz \quad \text{(D5)}$$

Minimization of γ_{site} with respect to $x(z)$ yields the z-dependent hybridization isotherm profile,

$$\frac{x(z)}{1 - x(z)} = c_tK_{bulk}\exp[-\upsilon_{sp}nc_s^0(z)] = \frac{x_{bulk}}{1 - x_{bulk}}\exp\left[-\frac{3\upsilon_{sp}nN_s}{2\Sigma H_0}\left(1 - \frac{z^2}{{H_0}^2}\right)\right] \quad \text{(D6)}$$

In contrast, when $F_{sp} < F_p$,

$$\gamma_{site} \approx F_0 + F_p + F_{mix} + \Delta F_{hyb} = F_0 + kT\frac{\upsilon_p n^2}{\Sigma}\int_0^{H_0}[1 + x(z)]^2{g_0}^2(z)\,dz + kT\int_0^{H_0} g_0(z)\,\{x(z)\ln x(z) + [1 - x(z)]\ln[1 - x(z)] - x(z)\ln(c_tK_{bulk})\}\,dz \quad \text{(D7)}$$

and its minimization with respect to $x(z)$ leads to

$$\frac{x(z)}{1 - x(z)} = c_tK_{bulk}\exp[-2\upsilon_p n^2[1 + x(z)]g_0(z)/\Sigma] = \frac{x_{bulk}}{1 - x_{bulk}}\exp\left\{-\frac{6\upsilon_p n^2 z}{\Sigma H_0}[1 + x(z)]\sqrt{1 - z^2/{H_0}^2}\right\} \quad \text{(D8)}$$

Equations D6 and D8 are the counterparts of the scaling expressions for the hybridization isotherms in a spacer-dominant brush (Section IV). The prefactors in front of the z-dependent functions in the exponents in eqs D6 and D8,

$$\frac{\upsilon_{sp}nN_s}{\Sigma H_0} \approx n\left(\frac{\upsilon_s}{a_s\Sigma}\right)^{2/3} \quad \text{and} \quad \frac{\upsilon_p n^2}{\Sigma H_0} \approx \frac{\upsilon_p n^2}{\upsilon_s N_s}\left(\frac{\upsilon_s}{a_s\Sigma}\right)^{2/3} \quad \text{(D9)}$$

match the corresponding expressions for $\Gamma(x_{eq})$ in eqs 33 and 31.

Using $c_p^0(z) = n[1 + x(z)]g_0(z)/\Sigma$ to account for the hybridization of the probes leads to

$$\frac{c_p^0(z)}{c_s^0(z)} \approx \frac{nz[1 + x(z)]}{N_sH_0\sqrt{(1 - z^2/{H_0}^2)}} > 1 \quad \text{(D10)}$$

at the periphery of the brush $z/H_0 \approx 1$ upon utilizing g_0 and c_s^0 given by eqs 47 and 51. Strictly speaking, this suggests a modification of the density profiles of the spacers and the probes. However, when the interaction terms F_{sp} and F_p are small compared to F_s, it is possible to use eqs 47 and 51 to specify the brush structure with the correction introduced previously for c_p^0. Moreover, in the limit $N_s/n \gg 1$, corresponding to $F_{sp} \gg F_p$, the condition $c_p^0(z)/c_s^0(z) \ll 1$ is fulfilled when

$$\frac{z}{H_0} \ll \left[1 + \left(\frac{n}{N_s}\right)^2\right]^{-1/2} \approx 1 \quad \text{(D11)}$$

Therefore, eqs D6 and D8 are asymptotically rigorous in the limit $N_s/n \to \infty$.

LA0616606